Role of electron spin dynamics and coupling network in designing dynamic nuclear polarization

Asif Equbal,[†] Sheetal Jain,[†] Yuanxin Li,[†] Kan Tagami,[†] Xiaoling Wang,[†,‡] and Songi Han[*,†,¶]

[†]*Department of Chemistry and Biochemistry, University of California, Santa Barbara, Santa Barbara, California 93106, United States.*

[‡]*Department of Physics, University of California, Santa Barbara, Santa Barbara, California 93106, United States.*

[¶]*Department of Chemical Engineering, University of California, Santa Barbara, Santa Barbara, California 93106, United States.*

E-mail: songi@chem.ucsb.edu

Edited by Geoffrey Bodenhausen and David Neuhaus

Abstract

Dynamic nuclear polarization (DNP) has emerged as a powerful sensitivity booster of nuclear magnetic resonance (NMR) spectroscopy for the characterization of biological solids, catalysts and other functional materials, but is yet to reach its full potential. DNP transfers the high polarization of electron spins to nuclear spins using microwave irradiation as a perturbation. A major focus in DNP research is to improve its efficiency at conditions germane to solid-state NMR, at high magnetic fields and fast magic-angle spinning. In this review, we highlight three key strategies towards designing

DNP experiments: time-domain "smart" microwave manipulation to optimize and/or modulate electron spin polarization, EPR detection under operational DNP conditions to decipher the underlying electron spin dynamics, and quantum mechanical modeling of coupled electron spins to gain microscopic insights into the DNP mechanism. These strategies are aimed at understanding and modeling the properties of the electron spin dynamics and coupling network. The outcome of these strategies is expected to be key to developing next-generation polarizing agents and DNP methods.

1. Introduction

Solid-state Nuclear Magnetic Resonance (NMR) spectroscopy is a powerful characterization technique with a broad application scope ranging from structural biology, biochemistry, molecular design, and catalysis to materials chemistry. NMR is a non-invasive technique that offers atomically detailed structural and dynamical information of crystalline and non-crystalline materials that may harbor significant disorder and/or heterogeneity. In spite of these merits, the intrinsically low sensitivity remains the bottleneck for expanding the utility of solid-state NMR for the characterization of surfaces and the detection and characterization of minor species, including low natural abundance isotopes or low population species. Dynamic Nuclear Polarization (DNP) is a rapidly evolving technique that can improve solid-state NMR sensitivity by several orders of magnitude using highly polarized electron spins (e) of a paramagnetic polarizing agent (PA).[1] DNP-NMR has provided unique access to chemical systems that are out of reach for conventional NMR characterization, including time-resolved structural studies of amyloid fibrils in their formation process, determination of the molecular structure of the reaction center in membrane proteins,[2–6] and multi-dimensional NMR of low-abundant NMR active nuclei such as ^{29}Si and ^{17}O in functional inorganic materials.[7–12]

However, there are inherent challenges in harnessing the full potential of DNP for solid-state NMR characterization. In particular, bio-molecular NMR cannot fully exploit the benefit of DNP given that the DNP efficiency is lower at high magnetic fields and under fast magic-angle spinning (MAS), both of which are important conditions for achieving high spectral resolution. Moreover, the requirement to use vitrified samples for DNP lowers the NMR spectral resolution, in part because of the properties of the vitrified sample itself, and in part because cryogenic operation $\sim$100 K relies on liquid nitrogen which limits reaching high MAS frequencies. DNP requires ^{1}H rich solvents for the diffusion of the polarization from the electron spins to the target sites. Hence, there are challenges in the utilization of DNP for materials not embedded in, impregnated with, or dissolved in ^{1}H-containing solvents.

The characterization of solvent-less materials demands innovation around the current DNP approaches that tend to be optimized for the polarization of abundant NMR active nuclei. In fact, even for archetypal ^{1}H rich systems that offer robust DNP performance, there still remains significant scope for increasing the DNP efficiency towards its theoretical limit.[1]

Here, we specifically focus on modeling the electron spin (e) coupling network and using "smart" microwave (μw) manipulation, with the ultimate aim of designing optimal PAs as well as DNP strategies. The effects of the nuclear spin (n) network and the glass-forming matrix are however beyond the scope of this review.

2. DNP of a ^{1}H-rich matrix

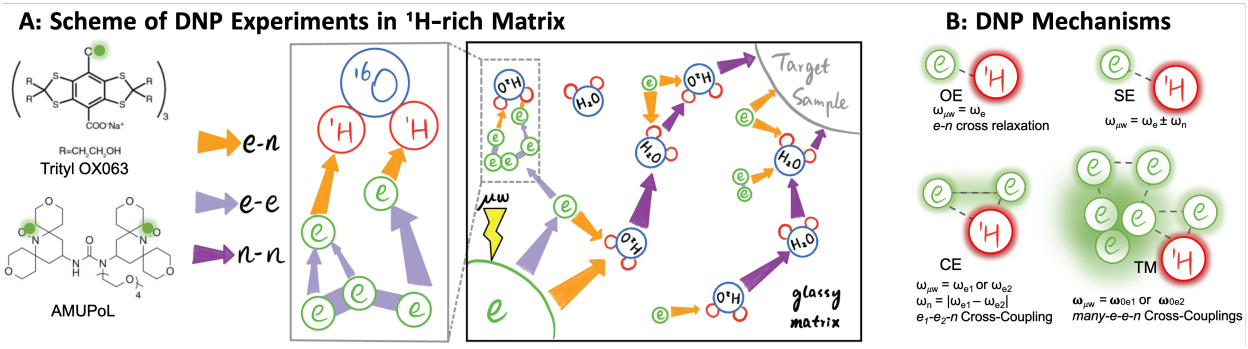

Figure 1: **A**: Schematic of polarization pathways for DNP of ^{1}H-rich solvent. The electron spin, ^{1}H of water, ^{16}O of water and target sample are represented as green, red, blue and grey circles, respectively. The e-n hyperfine couplings, e-e couplings and n-n couplings are displayed with differently colored arrows as indicated. **B**: Model system for four general DNP mechanisms: SE (e,n), OE (e,n), CE (2e,n) and TM (multi-e,n) with corresponding μw irradiation conditions.

The most common experimental approach to DNP is the selective saturation of the electron paramagnetic resonance (EPR) of the PA by μw irradiation, resulting in polarization transfer from e to n spins. A scheme of DNP experiments is illustrated in Figure 1A. Currently, the majority of DNP applications rely on nitroxide- or carbon-based PAs. The structures of the most commonly used PAs are included in Figure 1A, where the free electrons are marked with green circles. These PAs are dissolved in solvent mixtures such as

water-glycerol, water-DMSO or tetrachloroethylene (TCE) that form a glassy matrix upon vitrification and provide a ^{1}H spin-diffusion network. The NMR sample of interest is either dissolved in the PA-containing glass-forming matrix or is impregnated with it. DNP enhancement of NMR of samples impregnated with the PA-containing glass-forming matrix has proven to be a highly beneficial approach for surface characterization of materials, and is popularly referred to as DNP-Surface Enhanced NMR Spectroscopy (DNP-SENS).[12–16]

The polarization enhancement of the target sites in a glassy matrix relies on three major steps. First, the selective saturation of the EPR signals of PAs induces polarization transfer from the PA to nearby ^{1}H spins (orange arrows, Figure 1A). In the second step, the enhanced polarization is distributed among the ^{1}H spins of the glassy matrix via nuclear spin diffusion that allows the polarization to travel over distances of up to hundreds of nanometers (purple arrows, Figure 1A). The efficiency of spin diffusion is sensitive to the ^{1}H concentration in the solvent, which dictates the ^{1}H-^{1}H distance distribution, as well as to $T_1(^1\mathrm{H})$ (proton spin-lattice relaxation). Finally, cross-polarization (CP) using radio frequency (RF) pulses transfers the polarization from the abundant ^{1}H spins to the target lower γ (relatively insensitive) nuclei. As the polarization propagates through the solvent ^{1}H spins, sites inaccessible to the PAs can still be enhanced by this approach, while the undesired paramagnetic relaxation effects of the PAs on the target nuclear spin sites are minimized.[17,18]

3. Pertinent DNP mechanisms

DNP mechanisms can be broadly classified based on the number of coupled electron spins participating in the polarization transfer process (Figure 1B). These mechanisms can be further divided into coherent and incoherent processes depending on the relative strengths of the terms in the Hamiltonian of the system and their contributions to the spin relaxation rates. In a coherent mechanism, μw pulses are used to drive a particular transition in the e-n system, such that the corresponding polarization oscillates between e and n spins.

However, exploiting such coherent mechanisms requires further advances in μw technology (high power and pulse phase control) to be implemented at high B_0 field (discussed in section 4). Incoherent DNP is achieved by saturation of selected EPR transitions of the PA to achieve a steady-state nuclear spin polarization that is higher than at thermal equilibrium.

In this section, we will discuss pertinent DNP mechanisms within the incoherent regime. The earliest known mechanism is the Overhauser Effect (OE) that involves saturation of the allowed single quantum electron spin transition in a coupled e-n spin system followed by e-n cross-relaxation (Figure 1B).[19] Although very popular in liquids and conducting solids, OE has not been frequently observed in insulating solids under cryogenic conditions and high field due to the requirement of efficient e-n cross relaxation under cryogenic conditions. Another mechanism for enhancing nuclear spin polarization is the solid effect (SE) that relies on driving an e-n (forbidden) double quantum (DQ) or zero quantum (ZQ) transition, as illustrated in Figure 1B, and is applicable to many different types of solids.[20] However, these forbidden DQ and ZQ transitions become less probable at higher B_0, rendering SE inefficient.

Alternatively, the Cross Effect (CE)[21] and Thermal Mixing (TM)[22,23] mechanisms rely on (strong) e-e couplings (tens to hundreds of MHz) to induce simultaneous flip-flop-flip (triple-flip) transitions between two coupled e spins and a hyperfine coupled n (Figure 1B). For a triple- flip to occur, the difference of the EPR frequencies ($\Delta\omega_e$) of the two coupled e spins must match the nuclear Larmor frequency (ω_{0n}). Usually, if the EPR line is broadened by the g-anisotropies of the two coupled electron spins, CE occurs predominantly. On the other hand, if the dipolar (D) or exchange (J) coupling between electron spins broadens and shifts the EPR line by values greater than ω_{0n}, then TM typically becomes the dominant DNP mechanism.[22] In either mechanism, a large (Zeeman including g-anisotropy) polarization gradient ΔP_e across the EPR spectrum must build up under steady state upon μw irradiation to generate a net nuclear Zeeman polarization enhancement by the triple-flip. The magnitude and the rate of the e-n polarization transfer is determined by the integrated gradient ΔP_e and the e-e coupling strength (ω_{ee}), respectively.

To date, the search for PAs (especially for CE DNP) has been driven by optimizing parameters that have been empirically shown to improve DNP, including longer T_{1e} (electron spin-lattice relaxation times) to improve the ΔP_e,[24] mixed radical systems to maximize the triple-flip matching probability ($\Delta\omega_e = \omega_n$),[25–27] and stronger ω_{ee}.[28,29] Some of these developments have led to breakthroughs in DNP enhancement at high ($\geq$ 18.8 T) fields with PAs consisting of concentrated BDPA, HyTek, AsymPol and TinyPols.[26,28,30–32] Recent studies have shown that directly diagnosing and optimizing the topology of the *e*-*e* coupling network in a real sample (also including their relaxation rates, mutual *e*-*n* couplings, and EPR frequencies) provides a more complete approach for optimizing high field CE DNP.[28,33] EPR detection and quantum mechanical simulations are important tools in this pursuit.

In this review, we consider three strategies that can be used to design DNP experiments at high B_0 field, focusing on the promising CE DNP mechanism: (i) "smart" manipulation of the EPR transitions in time or frequency domain with carefully designed μw irradiation schemes to either optimize the polarization gradient for incoherent DNP, or to modulate the electron spin coherence in time domain; (ii) *in situ* EPR detection under operational DNP conditions (at present only possible in static samples), allowing observation of the polarization gradient under μw irradiation and the electron spin coupling network properties; and (iii) quantum mechanical calculations (numerical or analytical) of the coupled electron spin network to gain microscopic insight into different factors influencing DNP that cannot be experimentally manipulated, to predict and replicate experimental results. Studies relying on such tools and strategies have already led to several discoveries in DNP, as will be demonstrated with selected examples. We will next discuss each of these three tools.

4. Electron spin manipulation by "smart" microwaves

Contemporary commercial high-field DNP instruments powered by gyrotrons mostly rely on monochromatic continuous wave (CW) μw irradiation to saturate EPR transitions that

favour incoherent DNP mechanisms. However, time-domain modulation of μw irradiation would offer superior control of EPR transitions for DNP. We categorize time-domain DNP techniques into two approaches: (i) *Coherent DNP* that uses high-power μw pulses to coherently drive a certain transition of an *e-n* spin system resulting in nuclear polarization enhancement; and (ii) *Incoherent DNP* that relies on low-to-intermediate-power μw shaped pulses to induce broad-band and/or deliberately shaped, saturation of the EPR transitions in a selected frequency range. Here, time-domain modulation can compensate for the lack of μw power by saturating a larger number of EPR transitions in frequency domain, thereby recruiting a larger number of electron spins in DNP process. Future developments in μw instrumentation and DNP methodology will make these attractive options available for DNP spectroscopy. We will first discuss the instrumentation requirements for effective time domain manipulation, and then highlight coherent and incoherent DNP concepts.

4.1 Instrumentation

The choice of μw irradiation scheme is largely determined by the power, bandwidth, frequency agility, phase continuity, and pulse gating abilities of the available μw source. Coherent DNP requires high power (hundreds of watts) paired with nanosecond resolution of pulses. Incoherent DNP can be effective with much lower power (of the order of hundreds of milliwatts) delivered in CW mode or as pulse trains, with optional time-domain modulation, and greatly benefits from increased power. Gyrotrons are currently the μw source of choice for high-field DNP and deliver up to tens of Watts of power in monochromatic CW mode, which translates into nutation frequencies up to a few MHz. While this is not enough μw power for coherent DNP, gyrotrons are effective for achieving incoherent DNP. Recently, frequency-agile gyrotrons have become available that offer the option for sweeping the μw frequency over typically 120 MHz.[34,35] However, such gyrotrons span a limited frequency bandwidth (compared to the EPR line width and proton Larmor frequency) and cannot be used to achieve direct pulsing at the required nanosecond timescale to achieve coherent DNP.

Thus, state-of-the-art gyrotrons are a robust option for incoherent DNP at high field, but are unable to perform coherent DNP and EPR detection due their limited power, versatility and phase stability. Pulse slicing technologies to achieve external pulse gating of high-powered sources such as the free electron laser (FEL) exist and have been utilized for pulsed EPR.[36] However, FELs have not yet been developed for pulsed DNP applications.

Solid-state μw sources have complementary and orthogonal qualities for DNP applications compared to gyrotrons. They are compact devices driven by lower frequency μw signals, typically generated by a YIG synthesizer or voltage-controlled oscillator (VCO) operating at X-band (10 GHz) or W-band (35 GHz) frequencies. This low frequency signal is multiplied and amplified with an amplifier multiplier chain (AMC) to generate frequencies in the hundreds of GHz range. At a frequency range of 200 - 260 GHz, such device can produce up to 100 mW of μw power, which yields a nutation frequency of hundreds of kHz; with continuous gains in output power and maximum frequency. Critically, the solid-state source drivers are easily tuneable in frequency and amplitude with an accuracy of <100 Hz, and can be phase-locked to be exceptionally stable. Moreover, these sources can be combined with fast arbitrary waveform generators (AWGs) with a 2-10 GHz bandwidth, allowing for fine control over the amplitude, frequency, phase, and pulse gating with sub-ns time scales at the final high frequency output.[37] This capability to achieve modulation of a μw source using AWG in time-domain with high accuracy and speed provides opportunities to test new DNP methods, mechanisms, PAs, or samples. Furthermore, the precise control of μw irradiation offered by solid state sources allows EPR detection, making "in situ" EPR analysis of the DNP mechanism possible. Although solid-state sources do not produce sufficient μw power to be used for pulsed DNP, these are exceptionally versatile μw source drivers that can transform DNP approaches if paired with amplifier technology in the future.

Broadband amplifiers use low-power phase/frequency/pulsed/amplitude-controlled microwaves as input to produce high-power μw irradiation as output, ideally, with the same characteristic modulations. Currently, 2 types of amplifiers are being developed: gyroampli-

fiers and klystrons. Gyroamplifiers, developed by Temkin and coworkers,[38] can amplify the output power of typical solid-state sources to hundreds of watts and with sufficient bandwidth, but the generation of sufficiently long pulses (tens of μs) and their application to DNP requires further development. Klystron amplifiers have been demonstrated for DNP by Dupree et al.[39] They do not require an external magnet, and can output several watts of power. However, these amplifiers have a limited bandwidth of only about 0.4 GHz (at a 187 GHz carrier frequency), while scaling their output to higher frequencies is challenging due to their slow-wave design.

There is also great untapped potential to utilize resonant structures and optimum μw transmission pathways, as recently demonstrated by the pioneering work by Smirnov et al.[40] and Engelke et al.[41] to boost the effective nutation field, but this approach comes at the cost of bandwidth, frequency agility, sample size, as well as sample composition. Taken together, solid-state sources with AWGs are currently the most viable option to generate time-modulated microwave perturbations, and so develop next-generation DNP experiments, as well as to perform concurrent EPR characterization of the electron spin coupling network and polarization gradient under DNP conditions.

4.2 Coherent DNP

Over the last few years, Griffin and coworkers have tested a series of coherent DNP mechanisms for a coupled e-n system that in principle do not scale down with increasing B_0, unlike CE and SE. These DNP methods get inspiration from the coherence transfer processes routinely used in solid- and liquid-state NMR using RF pulses. A prime example of pulsed DNP is Nuclear Orientation Via Electron-spin Locking (NOVEL), introduced in short succession by Brunner et al.[42] and Henstra et al.[43] to rapidly transfer the polarization from photoexcited triplet electron spins to ^{1}H, and from paramagnetic holes in silicon-doped boron to ^{29}Si spins, respectively. This method is inspired by Hartman-Hahn cross-polarization (CP), which is an archetypal example of a B_0-independent heteronuclear polarization trans-

fer mechanism widely used in solid-state NMR. Recently, Griffin and coworkers[44,45] demonstrated the feasibility of using NOVEL for ^{1}H spins using the PAs of BDPA in polystyrene, sulfonated-BDPA and Trityl in water-glycerol solution at 0.35 T (X-band). This inspired the developments of schemes with lower μw power requirements such as off-resonance NOVEL,[46] as well as time-optimized μw pulse (TOP) irradiation induced DNP that rely on matching the effective field of the electron spin (in the rotating frame) to the nuclear spin Larmor frequency.[47] Such coherent DNP methods require high μw powers in short pulses to achieve broadband EPR excitation and spin-locking. Achieving this at high B_0 requires advanced microwave sources and instrumentation that are not yet commercially available. However, progress is being made in the development of new pulsed DNP methods, as discussed in a recent review by Tan et al.,[48] as well as the development of new μw source and amplifier technologies.[49,50]

4.3 Incoherent DNP

In contrast to coherent DNP, the efficiency of incoherent DNP can be dramatically amplified by time-domain pulse shaping, even when using modest power μw irradiation, compared to monochromatic CW μw irradiation, in particular to maximize the benefit of the triple-flip CE mechanism. The keys to achieving incoherent CE DNP are: (i) developing PAs with a high population of coupled (D or J) electron spins with a frequency difference that spans ω_{0n}, and (ii) generating a high polarization gradient between the pairs of electrons that satisfy triple-flip conditions across the EPR spectrum. The former requirement is dictated by the electron spin coupling network properties inherent to the sample and PAs, and is not influenced by low power μw irradiation. The latter requirement can be maximized using smart μw modulation to selectively saturate only part of an inhomogeneously broadened EPR spectrum in steady state to maintain a large ΔP_e. However, a certain PA architecture and relaxation characteristics are required to make selective saturation feasible and sustain the electron spin polarization gradient for sufficient time, as will be discussed.

The benefit of shaped μw irradiation was demonstrated for high field DNP and very low temperatures without MAS, first in the form of frequency modulation (FM) by Hovav et al. using μw irradiation at 95 GHz[51] and by Bornet et al. at 187 GHz.[52] In these studies, the μw frequency was swept periodically across large portions of the EPR spectra (with a spectral bandwidth comparable to the nuclear Larmor frequency) using a voltage-controlled oscillator, demonstrating higher enhancements. More recently, an AWG was utilized for μw pulse shaping in the time domain at 200 GHz to significantly boost the high-field DNP performance.[53] Here, instead of directly varying the frequency of the μw synthesizer (i.e., VCO or YIG), a periodic time-varying offset frequency of up to 1MHz/μs generated by an AWG is injected into the main μw carrier frequency via an IQ (Intermediate Quadrature Frequency) mixer, as illustrated in Figure 2A. This approach to achieve broadband irradiation with fast time-domain modulation has opened up the possibility of more sophisticated experiments.[54] Recently, a frequency agile gyrotron has also been developed that can directly sweep the output frequency by applying a time varying voltage to the gyrotron anode (shown in Figure 2B). This development is limited in speed and versatility, but can provide an order of magnitude greater μw power compared to an AWG driven solid-state source.[34,55,56]

The superior performance of AWG-DNP under static conditions encourages its application to DNP under MAS. However, the two cases are conceptually quite different. MAS bestows an additional time-dependence to the electron spin dynamics. Under MAS, the EPR resonances of electron spins undergo modulation in time due to their spatially anisotropic interactions such as *e*-*e* couplings and g factors (more discussion on this in the quantum mechanical section). Hence, CW μw irradiation saturates the polarization of different spin manifolds when their EPR frequency passes through and matches with the μw frequency, typically multiple times during the course of a rotor period τ_r. Under MAS, maintaining a large ΔP_e hence depends on the intrinsic properties of the radical (e.g., the magnitudes and relative orientations of g-tensors of biradicals). Electron spectral diffusion can further reduce the overall polarization gradient, rendering the implementation of AWG under MAS (Figure

2C) challenging. Recent developments have addressed this problem by using biradicals in which the two unpaired electrons have distinct g factors and anisotropies, and hence display frequency-separated EPR features, such as the covalent attachment, or a physical mixture of Trityl and TEMPO radicals.[25,57] Then, saturation will be induced within one radical, and not the entire EPR spectrum of the combined radical, thus helping to maintain a large ΔP_e. In order to restrict the saturation to the EPR resonance to one of the radical species, the sweep width of μw irradiation must be tailored to the width and shape of its EPR spectrum (as shown in Figure 2D).

The pulse sequence for an AWG-MAS DNP experiment designed to enhance the ^{1}H NMR signal is shown in Figure 2C, in which microwaves are swept across a frequency bandwidth multiple times within a given rotor period τ_r. AWG-MAS enhanced DNP has shown an improvement of up to 35% over CW DNP at 32 K for ^{1}H NMR in a solution of mixed Trityl-TEMPO biradicals using various waveforms generated by a solid-state source (Figure 2E).[54] Modulations with a frequency-agile gyrotron have shown a 24% improvement using a similar mixed Trityl-TEMPO biradical system at 90 K.[56] Moreover, quantum mechanical calculations predict that AWG-DNP can improve enhancements significantly compared to CW-DNP under conditions where T_{1e} is short relative to τ_r, and where high μw power is available (higher than has been so far achieved with state-of-the-art solid-state sources).[54] If T_{1e} is short relative to τ_r, saturation (or ΔP_e) is difficult to maintain for a sufficient time between the μw events (saturation) and the CE events (e-e-n triple-flip) that are time-separated in the course of the rotor period τ_r. Two time-separated μw and CE events within one rotor period are illustrated in Figure 3. Here, the relevant ΔP_e value at the CE event, illustrated in Figure 3A, is the difference between the amplitude of the solid and dashed blue lines. A small ΔP_e generates a small nuclear polarization during the CE event, as illustrated by a small (red) step function in Figure 3A. Rotor-synchronized AWG modulation of the μw frequency can help maintain a larger ΔP_e, by time-optimized fast and broadband saturation of the electron spin packets during rotor events (illustrated with rainbow-colored arrows

in Figure 3B). Maintaining a high ΔP_e at the e-e-n flip event generates greater net nuclear polarization, as illustrated by the larger (red) step function in Figure 3A, so that the CE DNP performance is enhanced. Hence, AWG-DNP can significantly enhance the DNP performance over CW DNP, especially under MAS when T_{1e}/τ_r is small. The fast sweeping of the μw frequency by AWG ensures that the μw saturation event occurs more frequently during τ_r, and closer in time to the CE event that generates a polarization transfer by triple e-e-n spin flips, and thus minimizes the deleterious effect of short T_{1e}.[54] This suggests that faster μw sweep rates render DNP more efficient. However, care must be taken because the optimal sweep rate will depend on the μw power and on the ratio T_{1e}/τ_r. More theoretical insights and experimental data are needed to derive general rules for how to optimize AWG-DNP under MAS. Nonetheless, AWG-DNP under MAS is an attractive option, especially when T_{1e} is short, as occurs at temperatures above 100 K.

Maximizing the electron spin polarization gradient is only half the story. Another critical parameter for DNP that requires attention is the coupled e-e-n polarization transfer rate, which scales down with increasing B_0 for typical PAs. The e-e interactions play a central role in determining the transfer rate. In fact, recent studies have shown that strengthening the electron spin couplings lead to significantly faster polarization transfer rates.[28,29] In systems with multiple coupled electron spins, the DNP mechanism may in fact transition from CE to TM as the number of e spins and the couplings among them increase. TM-DNP at high field is a relatively new phenomenon to consider for DNP under MAS, and needs further exploration. The EPR characterization of the coupled electron spins can help a better understanding of the process, and in turn develop strategies to efficiently manipulate and exploit a densely coupled many-electron spin network.[23,58–62] Overall, incoherent DNP using "smart" μw irradiation and carefully designed radical systems is a promising approach to improve the DNP performance by optimizing the electron polarization gradient across the EPR spectrum.

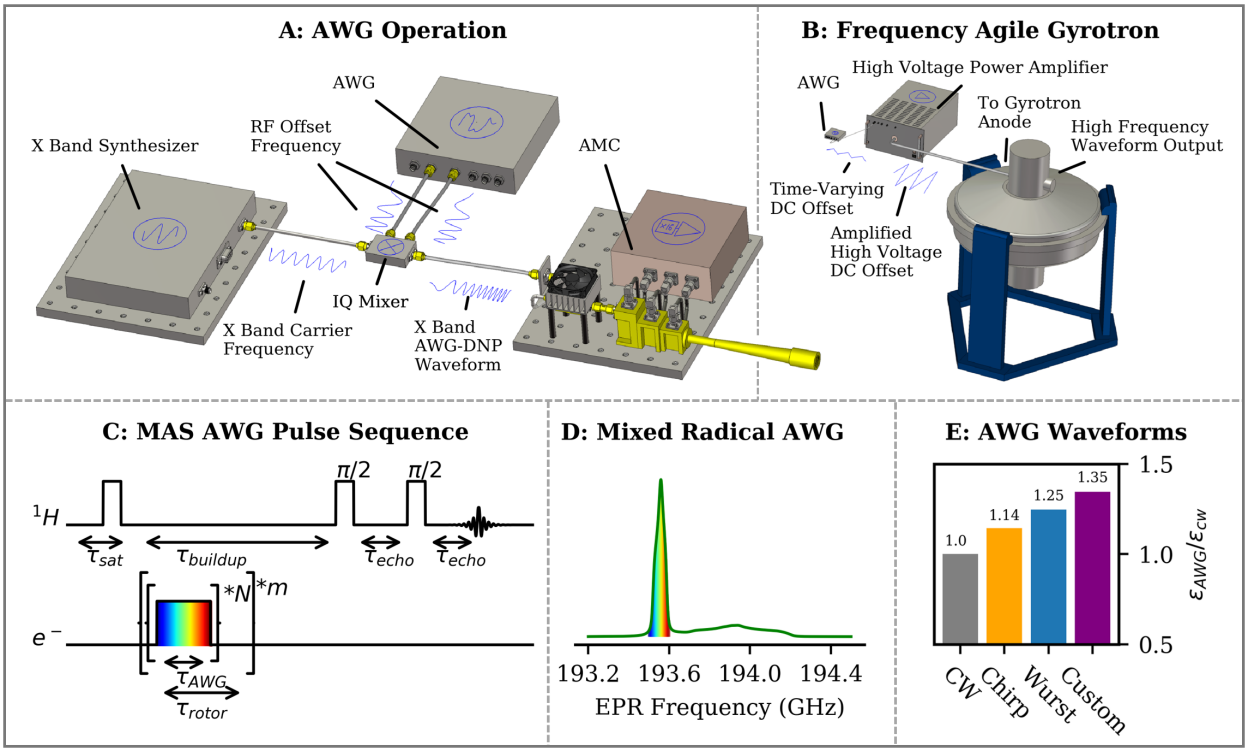

Figure 2: AWG-DNP: **A**: Basic components needed to carry out AWG-DNP. An X-band carrier frequency is first generated by a synthesizer, which is then mixed with a time varying RF frequency in an IQ mixer to produce the desired AWG-DNP waveform at X-band. This waveform is then multiplied to the desired high frequency in an amplifier multiplier chain (AMC). **B**: Rough schematic of wave-forming process with a frequency agile gyrotron. A time-varying DC offset voltage is generated by an AWG or function generator, which is then amplified to several kV by an amplifier and then fed to the anode of the gyrotron electron gun. By varying the voltage on the anode, the output frequency will change, and thus a voltage that varies in time will result in a swept μw output. **C**: Typical AWG-DNP experiment. During the buildup period, the μw frequency is rapidly ramped up and down multiple times in each rotor period. **D**: Typical frequency sweep in an MAS AWG-DNP experiment overlaid on the EPR profile (or electron spin density) of a mixed radical. AWG-DNP more effectively recruits the spins of the narrow line radical in DNP. **E**: ^{1}H DNP enhancement comparison of various AWG waveform at 3 kHz MAS, 7 T and 32 K. Figure E is adapted from reference[54] with permission.

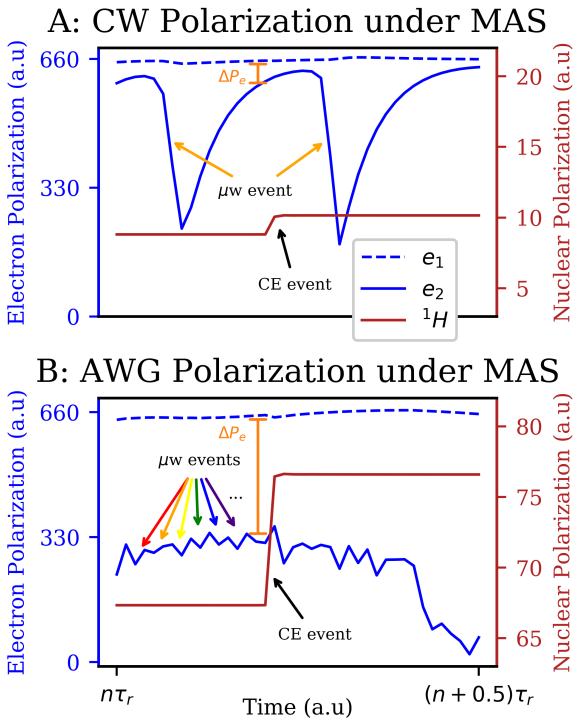

Figure 3: **Spins polarization trajectories.** Numerically simulated electron (blue, left y-axis) and nuclear (red, right y-axis) spin polarization trajectories measured for a single crystal orientation of e_1-e_2-n ($n = {}^1$H) spin system where e_1 and e_2 mimick Trityl and TEMPO, respectively. The polarizations are plotted for half a rotor period for steady-state conditions for e spins using **(A)** CW, and **(B)** AWG (linear chirp, with $\tau_r/\tau_{AWG} = 80$ and frequency bandwidth of 100 MHz) μw irradiation. The polarization was sampled every 5 μws, corresponding to τ_{AWG}. MAS was set to 2.5 kHz and $T_1(e_1) = T_1(e_2) = 0.1\tau_r$. Adapted from reference[54] with permission.

5. EPR Spin Dynamics Analysis

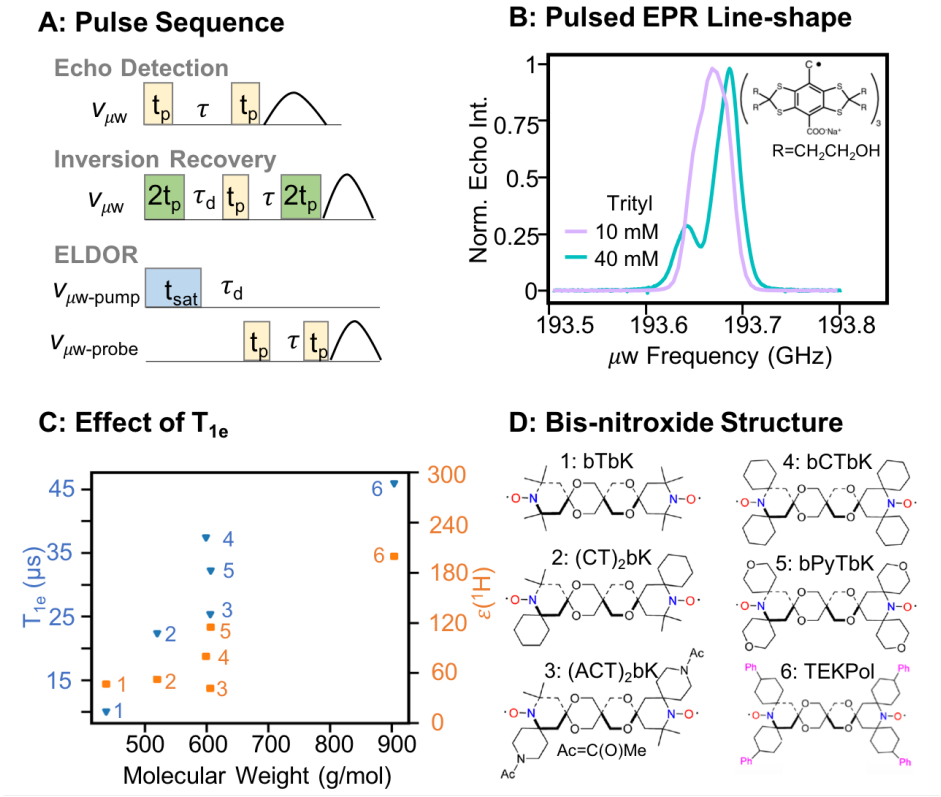

Figure 4: **A**: Pulse schematics for EPR experiments. **B**: Echo detected EPR spectra of Trityl-OX063 at 7 T.[61] **C**: T_{1e} (measured at W-band, marked with blue symbols) increases with the molecular weight of a radical (tested up to 905 amu) which results in higher DNP enhancement (measured at 9.4 T, orange symbols).[24] **D**: Structures of bis-nitroxide radicals in **C**. Panels B, C and D are reproduced and modified with permission with modifications from references[61] and[24] respectively.

The efficiency and viability of DNP mechanisms rely heavily on the electron spin properties of the PA. Hence characterization of electron spin parameters is critical to understanding and improving the triple-flip DNP mechanism. Current diagnostics of DNP mostly rely on the analysis of the nuclear spin dynamics (measurements of NMR signal enhancement) as a function of μw irradiation parameters, such as resonance frequency, power and irradiation time. Although the *e*-*e*-*n* transfer can be modified by effects of nuclear spin diffusion involving the bulk solvent ^{1}H nuclear spins, NMR signal enhancements provide incomplete insight into the *e*-*e*-*n* transfer process. Clearly, insight into the spin dynamics of both the electron

(the source of polarization) and the nucleus (the recipient of polarization) is needed for a comprehensive understanding of processes underlying DNP. Recent studies showed that the direct characterization of EPR spin dynamical properties of PAs under DNP conditions can exhibit surprising or even counter-intuitive features that will foster deeper insight and further developments.[61,63–66] Here, we demonstrate three different kinds of EPR data that aid in DNP studies: the CW and echo-detected EPR lineshape (i.e., the detectable electron spin population vs. resonance frequency/field), the electron spin relaxation rates and the electron spin polarization profiles under μw irradiation obtained by pump-probe experiments. These experiments are vital to gain insight into the *e*-*e* coupling network and its effects on the DNP mechanisms. We will present archetypal studies that showcase this point.

5.1 EPR lineshape analysis

CW EPR lineshape analysis combined with pulsed EPR techniques (Figure 4A) and DFT (Density Functional Theory) calculations can be used to obtain the g-anisotropy, intramolecular *e*-*e* dipolar and J coupling, *e*-*n* hyperfine coupling, as well as the zero field splitting parameters of many-electron spin PAs. Several studies relied on solution-state CW EPR line- shape analysis at X-band (0.35 T) to quantify the *e*-*e* J couplings in various biradical PAs.[67–69] Surprisingly, it was found that different enantiomers of a mixed trityl-nitroxide radical can have highly different J couplings ($\sim$196 and $\sim$6 MHz) that resulted in dramatically different DNP enhancements (7 and 40, respectively at 18 T).[70] Further discussions on the role of *e*-*e* dipolar and J couplings in biradicals for tuning their DNP performance will continue in section 6.

The CW EPR lineshape is not weighted by relaxation effects. Therefore, CW EPR does not provide direct insights into DNP-active (that can be saturated by μw irradiation) versus DNP-passive (that cannot be saturated) electron spin populations. In contrast, an echo-detected lineshape is modulated by electron spin relaxation times (T_1 and T_m), such that the spectrum is dominated by the slow relaxing electron spins that can likely be saturated by

μw irradiation. Therefore, an echo-detected EPR spectrum provides a representation of spin packets that can contribute to DNP experiments. In a recent study, echo-detected pulsed EPR experiments aided in the discovery of ^{1}H TM DNP with Trityl-OX063 (between 10-120 K) by revealing an asymmetric EPR lineshape that betrays the presence of heterogeneous spin populations – a condition required for TM, as theoretically predicted by Karabanov et al.[58,61] The asymmetry was a result of an intrinsic tendency of Trityl-OX063 to cluster at radical concentrations exceeding tens of millimoles/liter in a water-glycerol or DMSO solvent (Figure 4B).

5.2 Role of electron spin relaxation dynamics

In DNP, there is a tug of war between μw saturation and electron spin relaxation. Specifically, the selective saturation of an inhomogeneous EPR spectrum can give rise to a large electron spin polarization differential, ΔP_e, while T_{1e} relaxation pushes the polarization back towards its thermal equilibrium, thus reducing ΔP_e. Short T_{1e} rapidly reduces the polarization gradient and can lead to low DNP efficiency. This has been the key argument of a study by Ouari, Emsley and co-workers who developed a series of bis-nitroxide radials of the family of bTbk and TEKPOL exhibiting long T_{1e} that correlated with higher DNP enhancements (Figure 4C).[24,71] The strategy was to increase the bulkiness or the molecular weight of nitroxide-based PAs, and in turn slow down their motional dynamics to yield longer T_{1e} with a more rigid molecular framework near the radical center (Figure 4D). The T_{1e} values of the PA varied from 10 to 45 μs ($\sim$ 15 mM PA concentration, at 100 K and 3.5 T). The DNP enhancements measured at 100 K, 9.4 T and 15 kHz MAS, showed a direct correlation between T_{1e} and enhancement. Increasing T_{1e} increased the observed DNP enhancement. However, long T_{1e} can also induce the detrimental effect of nuclear depolarization under MAS (explained in section 6). We hence assume that there is an optimum regime for T_{1e} that should be long enough to maintain saturation, but short enough to replenish electron spin polarization after each rotor event, to avoid the undesirable nuclear depolarization effect

under MAS.[72]

It is worth noting that T_{1e} can be highly field dependent, underscoring the importance of measuring T_{1e} under DNP operating conditions.[66] Additionally, T_{1e} may vary significantly across a heterogeneously broadened EPR-line.[73] Identifying the spectral heterogeneity of T_{1e} is especially relevant for DNP if two distinct spin populations are strongly overlapping, or if one of them is spectroscopically invisible due to fast relaxation, while its presence still influences the DNP mechanisms. The comparison of CW and pulsed EPR spectra can reveal the presence of fast relaxing electron spin populations. One such example was demonstrated with the *truncated*-CE (*t*CE) DNP generated between a slow relaxing (narrow-line) Trityl radical and a fast relaxing radical cluster whose spectrum was severely broadened.[66] The discovery of *t*CE that had a similar appearance as OE DNP according to the NMR-measured DNP profile alone reinforces the importance of the measurement of electron spin dynamics in deciphering underlying DNP mechanisms.

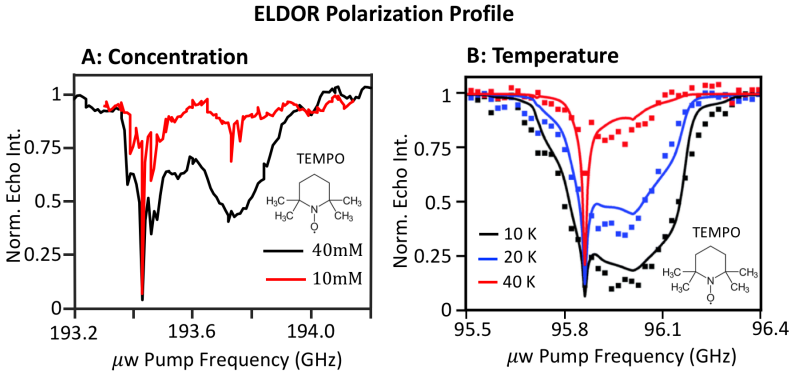

Figure 5: **A**: Concentration dependent ELDOR spectra of 10 mM and 40 mM TEMPO acquired at 4 K and 6.9 T with a probe frequency set to 193.45 GHz. A larger width of saturation at higher concentration implies larger electron spectral diffusion (eSD) driven by the stronger *e*-*e* couplings. **B**: Temperature dependent ELDOR spectra of 40 mM TEMPO acquired at 3.3 T and at variable temperatures: 10, 20 and 40 K. Larger width of saturation (or larger eSD) at lower temperatures is a manifestation of longer T_{1e} at lower temperatures. Panels A and B are reproduced and modified from references[74] and[75] respectively with permission.

5.3 Characterizing the *e*-*e* coupling network

DNP mechanisms and their efficiency strongly depend on the topology of the *e*-*e* coupling network and on the number of coupled electron spins participating, as illustrated in Figure 1B. The *e*-*e* coupling in a dilute (sub mM) bi- or tri-radical can be obtained using a combination of EPR measurements and DFT calculations. However, determining the topology of the coupling network in a concentrated radical system is not straightforward, especially because in a typical DNP experiment the PA molecules (used at concentrations of 10-50 mM) cannot be treated as systems of isolated electron spins. Additionally, the inter-radical couplings between electron spins can adopt uneven spatial distributions throughout a vitrified sample depending on radical-solvent and radical-radical (chemical and physical) interactions. To uncover properties of the *e*-*e* coupling network, we turn to two-dimensional pump-probe pulsed EPR measurements. The idea is to perturb the electron spins by mimicking the effect of microwave irradiation under DNP conditions, and then detect the resulting electron spin polarization that is dictated by the *e*-*e* spectral diffusion across the EPR line.

In a pioneering study, Hovav, Feintuch, Vega and Goldfarb introduced multi-frequency pump-probe Electron-Electron Double Resonance (ELDOR) measurements as a means of studying the *e*-*e* coupling network under DNP conditions.[76] The pump channel saturates the electron spin polarization to emulate the μw irradiation condition used in DNP experiments. The probe channel measures the polarization of electron spins at the selected probe frequency. This measurement reveals the role of electron spectral diffusion (eSD), which results in the spread of saturation across a wide frequency range that exceeds the bandwidth of the μw pulse. The saturation of spins via eSD is governed by the combined effect of the *e*-*e* coupling strengths (that determine the *e*-*e* flip-flop transition rate) and electron spin relaxation. Figure 5A shows ELDOR polarization profiles measured at 4 K and 6.9 T for a fixed probe frequency (193.45 GHz), while the μw pump frequency is varied through the complete EPR spectrum, for 10 and 40 mM TEMPO dissolved in water-glycerol. The eSD becomes dominant when inter-radical coupling is large (at 40 mM), demonstrating that eSD

is a qualitative indicator of the e-e coupling network. The extent and width of electron spin saturation also increases with T_{1e}, e.g. at lower temperatures. Figure 5B shows ELDOR polarization profiles of 40 mM TEMPO at a fixed probe frequency (95.86 GHz), acquired at three different temperatures, 10, 20 and 40 K, in a 3.3 T field. Clearly, eSD is more prominent at 10 K as revealed by the wider saturation dip compared to higher temperatures.

A complete two-dimensional electron spin polarization profile can be generated by measuring ELDOR profiles at different probe frequencies and by deconvoluting the relative contributions of different DNP mechanisms. Hovav et. al. developed a numerical model to use the two-dimensional ELDOR polarization profile to reconstruct the DNP frequency/field profile.[75] The model provided critical insights in distinguishing the direct CE (where ΔP_e is achieved by direct μw irradiation of one the two electrons inducing CE) and the indirect CE (where ΔP_e between the two electrons is generated as a result of eSD and not via direct irradiation). It was revealed that indirect CE is the major mechanism responsible for bulk DNP at all three temperatures.

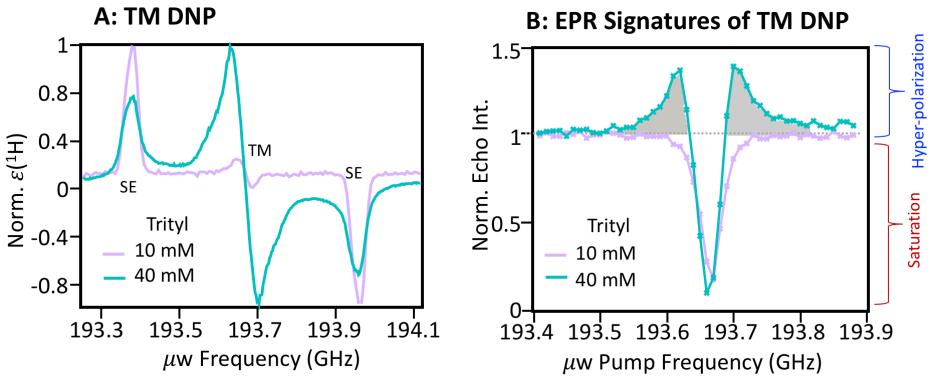

Figure 6: **A**: DNP frequency profiles of 10 mM (violet) and 40 mM (mint) Trityl-OX063 at 20 K and 6.9 T. The prominent ^{1}H DNP mechanism undergoes a crossover from SE to TM at the higher concentration of Trityl. **B**: The ELDOR profiles measured for the two concentrations near the Trityl-OX063 center frequency. Hyperpolarization at 40 mM (shaded in gray) reveal the EPR signatures of TM DNP. The figures are reproduced and modified from reference[61] with permission.

Recently, we observed ^{1}H TM DNP using a narrow-line (i.e., with a g-anisotropy smaller than ω_{0n}) water-soluble Trityl-OX063 radical at 7 T. Surprisingly, the DNP mechanism

crosses over from SE to TM with increasing concentration of Trityl-OX063 between 10 and 40 mM (Figure 6A). ELDOR measurement served as a powerful diagnostic tool to unambiguously identify a TM signature in a strongly coupled spin system, as had been numerically predicted by Vega and co-workers.[77] Their key prediction was the generation of the hyperpolarization (or cooling) of selected electron spin resonances under the effect of TM DNP, when the μw pump frequencies is set at some distance from the probe frequency.[61] Figure 6B shows overlaid ELDOR polarization profiles (normalized with respect to the Boltzmann polarization) for two different Trityl-OX063 concentrations. Clearly, in the sample containing 40 mM of the PA, TM is the dominant DNP mechanism. An increase in the polarization of electron spins above the thermal Boltzmann distribution is observed when the μw pump frequency is set at an offset with respect to the probe frequency. The hyperpolarized electron signal is highlighted in gray. When μw pump and probe frequencies are close, only saturation of the EPR signal (shown as a dip in intensity in the ELDOR profile) is observed for both PA concentrations.

5.4 Underlying DNP Mechanism in BDPA

A recent study applied EPR line-shape and ELDOR analysis to identify the DNP mechanism of concentrated 1,3-bisdiphenylene-2-phenylallyl (BDPA) in vitrified *ortho*-terphenyl (OTP) or polystyrene solutions, a condition that showed promising DNP performance at high magnetic fields and under fast MAS conditions.[32,78,79] OE DNP was the mechanism proposed for these insulating (non-conductive) systems under cryogenic conditions based on the shape of the DNP field profile, as shown in Figure 7A. However, the mechanism of OE in insulating-solids/BDPA is subject of some debate, as the nature of the dynamics required for cross-relaxation under these conditions has not been verified experimentally. Recently, we presented an alternative explanation that the dominant underlying DNP mechanism of ^{1}H NMR enhancement in BDPA is TM.[62] The high-field echo-detected EPR line shape was found to be asymmetric (see Figure 7B), similar to the EPR spectrum of Trityl prepared for

DNP (discussed above). Moreover, the echo-detected EPR line-shape at varying temperatures confirmed the co-existence of both clustered and isolated forms of BDPA, with each population displaying highly different relaxation rates. Notably, broadened EPR components disappear at higher temperature, presumably due to faster relaxation. Additionally, ELDOR experiments demonstrated that hyperpolarized electron spin polarization can be generated by off-resonant μw irradiation under DNP conditions (Figure 7C). An intensity of EPR signal above the Boltzmann level (normalized to 1) implies hyperpolarization of electron spins. This is highlighted in gray. These observations reveal that DNP with concentrated BDPA as the PA is critically dependent on multi-electron spin coupling, supporting the underlying mechanism as being TM DNP, which, unlike OE DNP, relies on a strong *e*-*e* coupling network.

Resolving the underlying DNP mechanism is critical to developing the design of the PAs, and to define the desired capabilities of μw instruments for DNP experiments. If the DNP mechanism is known, the utilization of DNP for applications can be accelerated. The discussed examples showcase the merit of EPR detection under DNP conditions as an efficient tool to rationalize and design DNP experiments. Advances in μw technology such as amplifiers and high-power pulse slicers will further promote EPR diagnostic capabilities in the future.[80]

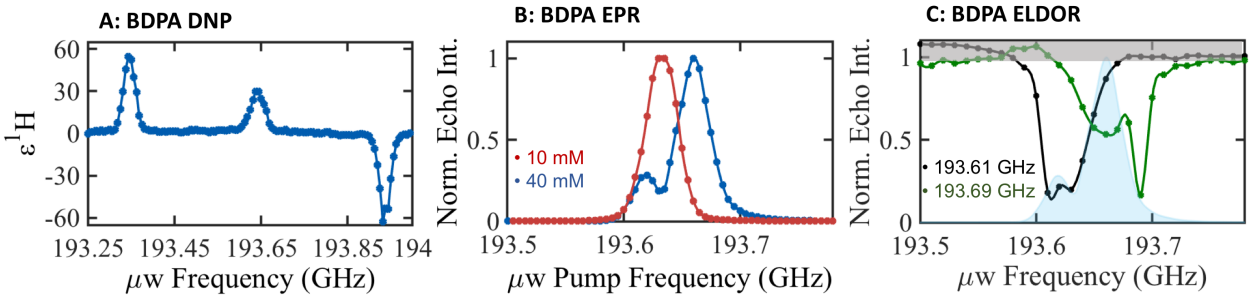

Figure 7: **A**. DNP frequency profile of 40 mM BDPA in OTP at 20 K and 7 T. **B**. Echo detected EPR spectra of 10 mM and 40 mM BDPA. **C**. ELDOR spectra of 40 mM BDPA at two probe frequencies, depicting the hyperpolarization (shaded in gray) of electron spins– a signature of TM DNP.[62]

6. Quantum Mechanical Modeling of Spin Physics

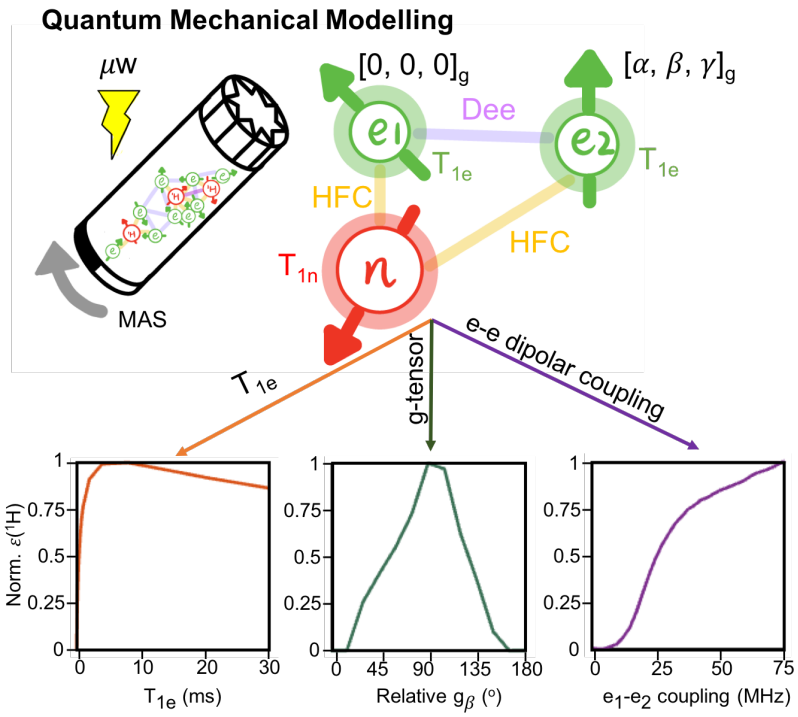

Figure 8: Quantum mechanical modeling of T_{1e}, relative g-tensor orientations and dipolar coupling in bis-nitroxide radicals under 25 kHz spinning in a field of 18.8 T using 0.5 MHz μw nutation frequency.

The DNP pathways and their efficiencies depend on a multitude of different intertwined parameters. Quantum mechanical (numerical) simulations offer a unique handle to selectively monitor the effect of different spin dynamics parameters and to dissect and understand DNP at a microscopic level.[27,33,81–83] Figure 8 illustrates the model of a PA (bis- nitroxide for CE DNP) with parameters including the relative g-tensor orientation, the *e*-*e* dipolar coupling between two coupled electron spins, as well as T_{1e}. The calculation of the proton enhancement $\epsilon(^1\text{H})$ for a typical bis-nitroxide under MAS predicts that: (i) a sufficiently long T_{1e} (i.e., above a threshold) is critical for efficient DNP, but an excessively long T_{1e} becomes deleterious, (ii) there are preferable relative g-tensor orientations between two coupled electron spins that maximize CE DNP, and (iii) generally, stronger *e*-*e* dipolar couplings enhance the DNP performance (up to a threshold value), largely validating experimental observations.

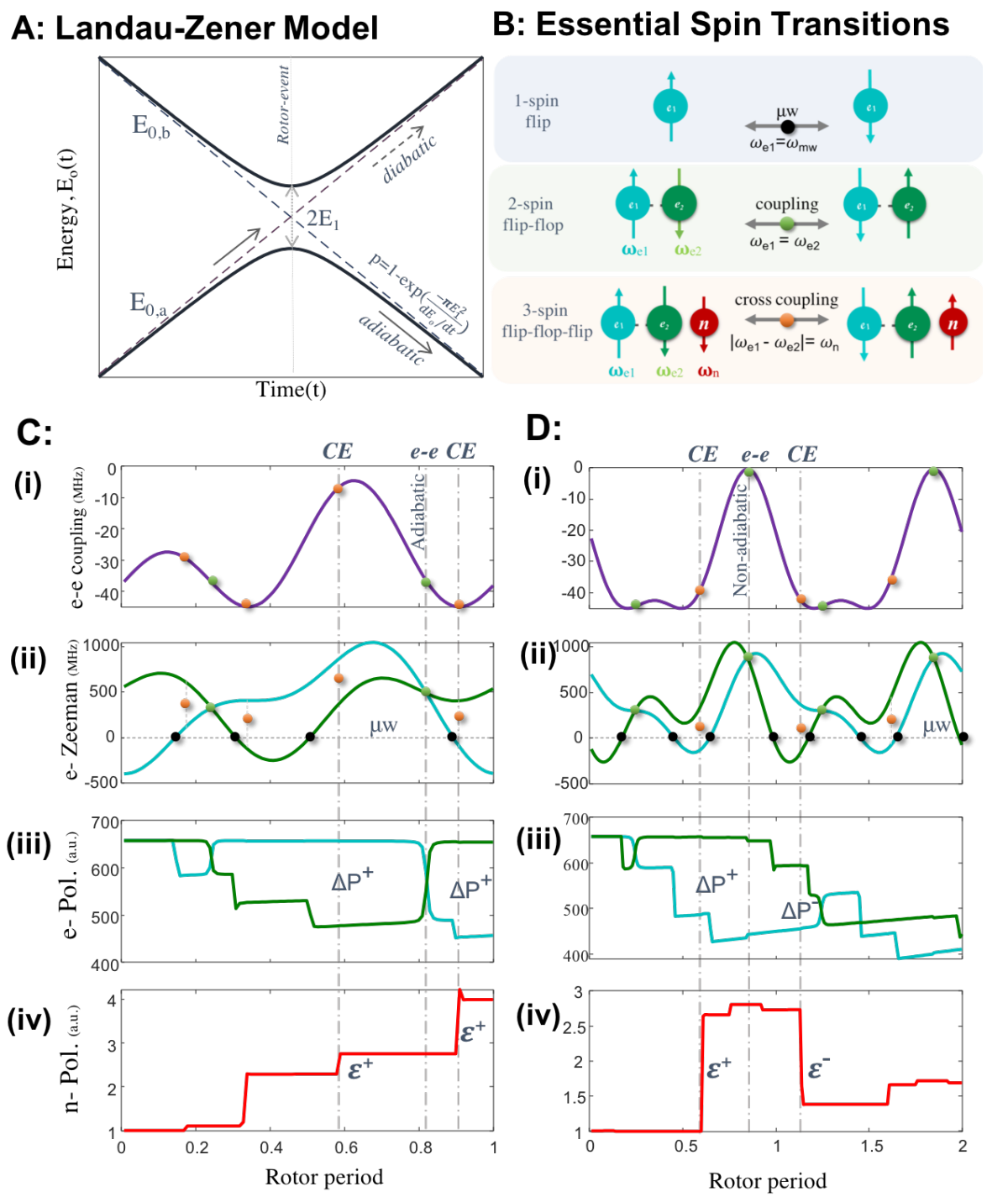

Figure 9: **A**. Landau-Zener population transition model used to rationalize spin dynamics under MAS. **B**. Schematic representation of essential spin transitions involved in CE DNP. **C**. Plot of *e-e* coupling (panel *i*) and *e*-Zeeman energies in rotating frame (panel *ii*), the electron and nuclear spin polarizations (panels *iii* and *iv*, respectively). The rotor events μw, *e-e* and CE are marked with black, green and orange symbols. The *e-e* couplings at the green *e-e* rotor events are large and therefore corresponding transitions are adiabatic. **D**. Similar to **C** but for a different crystallite orientation that leads to inefficient DNP. A non-adiabatic *e-e* event impedes the net DNP enhancement. The energies and polarizations were calculated using SpinEvolution package26

These profiles were calculated by varying a selected parameter (shown along the x-axis) while keeping all other parameters constant (typical for bis-nitroxides).[28,69,83] Notably, EPR measurements of spectral (J coupling, g-tensor) and relaxation (T_{1e}, T_{2e}) properties offers critical input to accurately carry out the relevant DNP simulations.

In this section, we will focus on how quantum mechanical analysis can enhance our understanding of the role of the DNP parameters. We will focus on CE DNP, which is the most accessible mechanism for MAS DNP. Notably, the widely used average Hamiltonian theory or Floquet theory cannot be straightforwardly applied to study time-dependent interactions involving electron spins under MAS, as the strength of these interactions are much larger than the MAS frequency itself.[84]

6.1 Landau-Zener Model

A major development in the (quantum mechanical) understanding of the CE DNP mechanism under MAS came from the description of dynamic electron spin transitions using the Landau-Zener (LZ) model, as delineated by Tycko and Thurber,[85] and subsequently by Mentik-Vigier et al.[86] Their studies contributed to unraveling the distinctions between of MAS DNP and static DNP. Under MAS the essential spin transitions leading to μw excitation and other spin flip-flop events are separated in time (unlike under static conditions) because of energy modulation in time owing to anisotropic interactions of the electron spins (i.e., the g tensor anisotropy and dipolar *e*-*e* couplings). The energy modulation causes a series of time-dependent and periodic resonance conditions (a.k.a. rotor events) where spins may transition from one state to another. The changes of spin populations between energy states at a rotor event where a resonance condition is met can be analyzed by the LZ model. According to this model, the probability for population exchange (p) at each rotor event depends on the rate of change of the energy of the states ($\frac{dE_0}{dt}$) and the magnitude of the

perturbation (E_1) at the rotor event according to the following equation:

$$p = 1 - exp(-\pi * E_1^2/(\frac{dE_0}{dt})). \quad (1)$$

Figure 9A represents a level anti-crossing (rotor event) in a two energy-level system. The dashed lines represent the energies of the diabatic states (diagonal terms of the Hamiltonian, E_{0a} and E_{0b} not including the perturbation term). The solid lines represent the energies of the adiabatic states of the Hamiltonian (eigenvalues of the full Hamiltonian, including the perturbation term). The rotor event is said to be diabatic if there is negligible exchange of the spin populations between the energy states, while an adiabatic transition refers to a complete exchange of the spin populations between the states (see Figure 9A). These concepts are pedagogically explained in a recent review article by Ivanov and coworkers.[87] As mentioned above, CE involves two essential transitions: (i) μw event: selective saturation of one of the electron spin polarizations in resonance with the irradiating μw frequency (i.e. $\omega_{e_i} = \omega_{\mu w}$), and (ii) CE event: simultaneous triple-spin flip of *e*-*e*-*n* at the CE resonance condition (i.e. $\omega_{e_1} - \omega_{e_2} = \pm\, \omega_n$). There is another very critical transition, the *e*-*e* event that occurs when the two electron spins become degenerate ($\omega_{e_1} = \omega_{e_2}$), leading to the partial or complete exchange of polarization between e_1 and e_2 spins. These transitions or the rotor events are illustrated in Figure 9B.

Using the basic understanding of the LZ model, we now address an important question: what determines the DNP efficiency of a polarizing agent? The DNP enhancement is highly orientation dependent, and encoded in the energy trajectories of the energies of the states which determine the sequence of the rotor events. Additionally, the relaxation time constant T_{1e} relative to the rotor period (τ_r) determines whether the effect of the different rotor events can add up constructively or not. Very short T_{1e}/τ_r will relax the system back to thermal equilibrium in between the rotor events.

We illustrate these nuances using two selected orientations, one leading to efficient DNP

and the other to inefficient DNP. Figure 9C-D maps the e-e coupling energies (panel i) and Zeeman energies in the rotating frame (panel ii) of two electron spins (e-e-n with $n = {}^1$H spin system) in the μw rotating frame for an e-e-n crystallite orientation that leads to high (C) and low (D) DNP enhancements. The modulation in panel (i) results from the dipolar anisotropy of the e-e coupling. The coupling energy spans the range $[\frac{-D}{2} + J, D + J]$. The modulation in panel (ii) results from the g-anisotropy of the electron spins. Panels (iii) and (iv) map the polarization profiles of the two electrons and the nucleus, respectively.

The rotor events, involving one (μw event), two (e-e events) and three spins (CE event), are marked by black, green and orange symbols, as their resonance conditions are satisfied at different time points within a rotor period. Essentially, a μw event (time point where the Zeeman energy of one of the electrons becomes zero, (marked by horizontal dotted lines) in the μw rotating frame generates a polarization difference between the two electron spins (panel ii). The change in the polarization of the two electron spins can be monitored in panel (iii) of Figure 9C-D.

$$\text{perturbation strength of CE transition} \approx \frac{\omega_{e_i e_j}(\omega_{e_i n} - \omega_{e_j n})}{\omega_{0n}} \tag{2}$$

The nuclear polarization enhancement occurs with the triple e-e-n spin flip transition, here referred to as the CE rotor event, in a step-function by an amount that is proportional to ΔP_e accumulated prior to this event (also illustrated in Figure 4). These transitions are marked with orange symbols, where the difference of electron spin energies matches the nuclear Larmor frequency, i.e. 300 MHz for ^{1}H at 7 T (panel ii). The transition probability can be calculated using the LZ equation, where the perturbation E_1 depends on the product of the e-e coupling and the relative e-n coupling as shown in Equation 2. The corresponding step-wise buildup of nuclear spin polarization of the selected orientation under MAS is shown in panel (iv) of Figure 9C-D.

Maintaining high adiabaticity, especially for all e-e events in a rotor period, is key to achieving high CE DNP under MAS. A favorable e-e event leads to an exchange of elec-

tron spin polarization, provided that the instantaneous e-e coupling is large enough at the event.[85,86] This is important to maintain the electron spin polarization gradient, as well as to maintain the same sign of the polarization difference $\Delta P_e = P_{e_1} - P_{e_2}$ and the frequency difference $\Delta\omega_{0e} = \omega_{e_1} - \omega_{e_2}$. To understand this nuance, let us focus on the e-e event, which is interleaved between two CE events (Figure 9C, panel $ii - iii$) as highlighted with dashed vertical lines. Prior to the e-e event, the polarization difference ΔP_e between the two electrons with respect to their frequency difference $\Delta\omega_{0e}$ and the corresponding DNP enhancement is positive, ϵ^+ (Figure 9C panel iv). After the e-e event, the electron frequency difference changes the sign (i.e., the green symbol is higher and the cyan symbol is lower in energy). For the CE DNP to constructively add up, the polarization of the two electron spins should swap, so to maintain the polarization difference, and maintain its sign with respect to the frequency difference. This requires that the e-e event is adiabatic (i.e. $p \sim 1$ in Equation 1), contributed by a large e-e coupling at the event, as seen in Figure 9C. Then, a large DNP enhancement is achieved. In contrast, if the e-e event (highlighted with dashed line) is diabatic or non-adiabatic, as illustrated in Figure 9D panels $i - iv$, and the relative sign of ΔP_e and $\Delta\omega_{0e}$ is not maintained at the two different CE events (before and after the e-e event as highlighted), this can lead to self-cancellation effects for DNP. Also, the large ΔP_e is not maintained at steady state. Notably, even a single non-adiabatic e-e event can lead to poor DNP enhancement for the select orientation (Figure 9D, panel iv). In a nutshell, the sequence of the rotor events, the adiabaticity of these transitions and the relative T_{1e}/τ_r all contribute to the CE-DNP efficiency of a given crystallite or molecular orientation. An ideal PA will be one with maximum adiabatic transition probabilities for all e-e events in a rotor period, and is fulfilled for a large number of orientations in a powder ensemble.

6.2 Design of new polarizing agents.

A major research topic in MAS DNP has been the design and synthesis of biradicals that are more efficient at high B_0 and fast MAS frequency. In particular, the search for a bi-radical

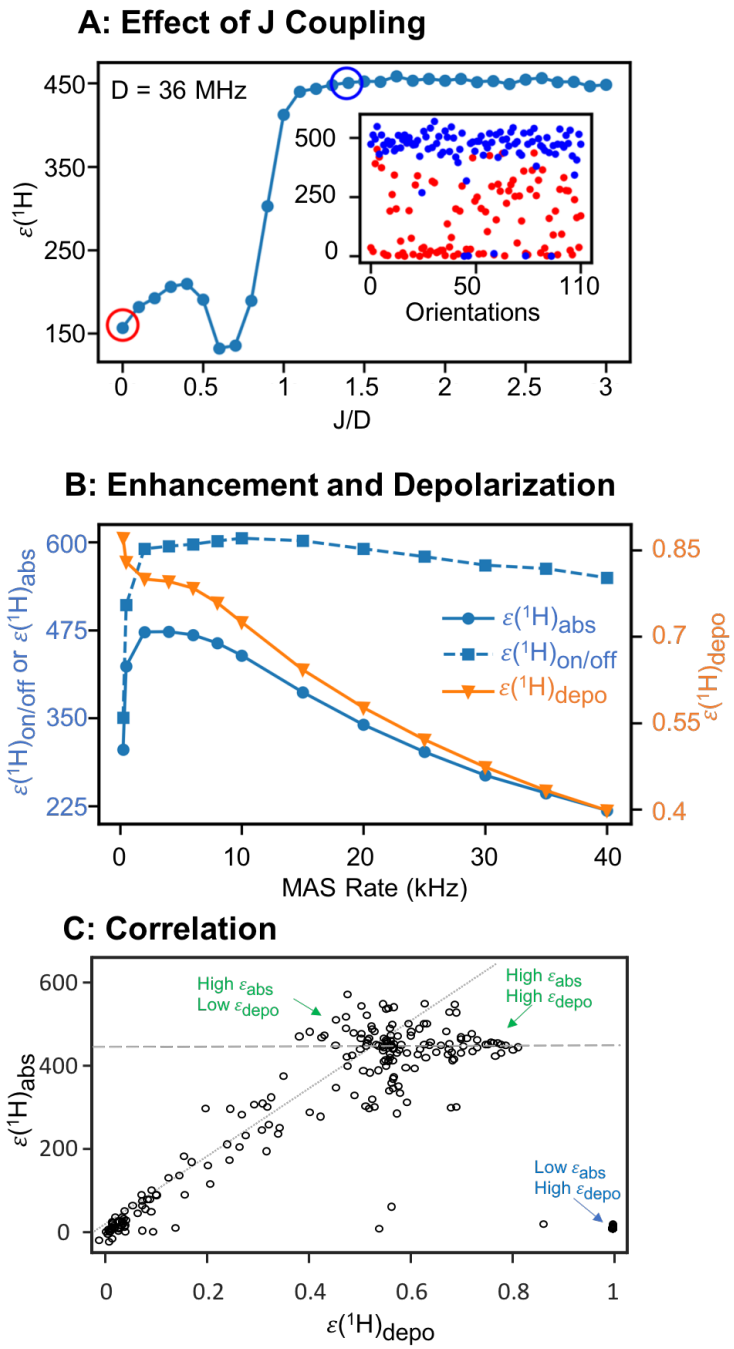

Figure 10: **A**. ^{1}H DNP vs. J/D in bis-nitroxide exhibiting the requirement of an optimal J/D for maximum enhancement. Non-optimal J/D of ∼0.7 results in strong interference in bis-nitroxides with perpendicular g-tensors. **B**. Measured ^{1}H DNP enhancement $\epsilon_{on/off}$ on left y-axis, and nuclear depolarization (ϵ_{depo}) on right y-axis for a powder sample. The more meaningful ϵ_{abs} is defined as $\epsilon_{on/off}{}^*\epsilon_{on/off}$. This shows that the factor $\epsilon_{on/off}$ overestimates the actual DNP enhancement. **C**. Numerically simulated correlation between enhancement and depolarization for 230 different crystallite orientations mimicking AMUPol spin parameters at 12.5 kHz MAS and 18.8 T field. Figure A is adapted from reference[33] with permission. Figure B was simulated numerically using SpinEvolution under 25 kHz spinning and 18.8 T field using 0.5 MHz μw nutation frequency.

with optimum *e*-*e* coupling has been an important research focus. Initially, the optimization of the biradicals was based on the optimization of the dipolar coupling and g-anisotropy through variation of the chemical linker connecting the radical centers. The aim was to optimize (i) the length of the linker and thereby the dipolar coupling and (ii) the rigidity of the linker to ensure an optimum relative orientation of the g-tensors of the two radical centers in the bi-radical. This design approach is further being refined by considering the role of exchange or J coupling.[26,28,69]

Sigurdsson, De Paëpe and coworkers have designed an asymmetric bis-nitroxide radical, AsympolPOK, to maximize the CE DNP efficiency while minimizing the depolarization effect; it is reportedly the best performing bis-nitroxide radical at 18 T to date.[28]

Recently, we discovered the importance of balancing the relative magnitude of J and D in a biradical for maximizing the enhancement in a powder sample.[33] This is illustrated in Figure 10A that shows simulated 1H DNP enhancements as a function of the relative J/D values in bis-nitroxide radicals. We discovered that not only the sum J+D, but also the ratio of J/D needs to be balanced (specifically in the range $1 < J/D < 2.5$) to achieve robust enhancement for all radical orientations.[33] The recently developed TinyPol PA is a very appropriate example to highlight the necessity of balancing J and D coupling. Compared to AMUPol, the TinyPol radical has a smaller linker, and therefore much enhanced dipolar coupling ($\sim$ 40 MHz). However, the J coupling ($\sim$ 22 MHz calculated using DFT) of a large number of conformers falls in a non-optimum regime ($J/D \sim 0.55$), hence rendering its performance far below that than initially expected. In fact, the key strategy to boost DNP efficiency at high B_0 and fast MAS is to enhance the ratio of the isotropic J coupling and the anisotropic D coupling between the CE-inducing electrons spins. This strategy minimizes the interference effects between the two interactions and maximizes the effective *e*-*e* couplings at all radical orientations, thus ensuring large adiabaticity for the *e*-*e* and CE rotor events. In all transitions, again, maintaining high adiabaticity is the key for achieving efficient DNP. The adiabaticity of CE rotor-events is the smallest in magnitude (relative to

other two rotor-events) as it is a second order perturbation term77 that is proportional to the product of e-e and the difference between two e-n couplings and is scaled down by the nuclear Larmor frequency (Equation 2).

Therefore, the adiabatic transition probability of the CE event becomes smaller with increasing magnetic field. The loss of adiabaticity of the CE event at higher field can be compensated for with an increase in the e-e coupling, as reflected in Equation 2.

6.2.1 Mixed Radicals

Given that the main source of EPR frequency modulation under MAS is the modulation of the g-tensor of the molecular orientation of the individual radicals (also referred to as crystallites), the rate of change in the energy ($\frac{dE_0}{dt}$) (Equation 1) increases linearly with the B_0 field and with the MAS frequency. Therefore, maintaining a large μw induced saturation at high B_0 field or fast MAS becomes challenging for a bis-nitroxide that has a g-anisotropy exceeding 1 GHz at high B_0. Comparatively, carbon-based radicals have smaller g-anisotropy, and are easier to saturate since they have a longer T_{1e}. Trityl and BDPA are the most common radicals in this category. Their g-anisotropies are smaller than the proton Larmor frequency, and hence the spectral density of these carbon-based radical monomers does not satisfy the ^{1}H CE DNP condition. However, this changes dramatically when there is significant inter-radical e-e coupling, presumably due to radical clustering, as discussed earlier in section 5. A novel idea was proposed by Griffin and coworkers to use a physical mixture combination of nitroxide and carbon-based radicals as a PA for maximizing CE DNP.[57] This idea worked because differences in the g-tensors between the nitroxide and carbon-based radicals as they have favorable relative g-tensors to fulfill ^{1}H DNP conditions,[57] while the carbon-based Trityl or BDPA radicals can be easily saturated, even at high B_0 fields, with only moderate μw powers of a few hundreds of milliwatts, rendering them favorable for DNP when used in combination with nitroxide radicals. The use of mixed radicals as PA has generated the best DNP performance to date at high magnetic fields, as demonstrated

by Emsley and coworkers in a recent report with a mixed BDPA – nitroxide radical PA.[26] Interestingly, the CE DNP efficiency of mixed radicals remains high even when the relaxation of the nitroxide spin is very fast because the role of the nitroxide radical is to provide enough EPR spectral bandwidth to encompass the occurrence of *e*-*e*-*n* triple-flips, while the saturation efficiency of the nitroxide radical in the context of a mixed radical is not a major factor that boosts DNP.[66] The DNP performance using mixed radical systems may be further enhanced by optimizing the electron spin densities and ratios of narrow and broad radicals, as proposed by Li et al.[27]

6.3 Depolarization effect under MAS

DNP enhancement is generally evaluated by comparing the NMR signal intensities under μw-*on* and -off conditions, i.e. ($\epsilon_{on/off}$). However, when evaluating the DNP efficiency, it is important to consider the effect of nuclear depolarization (ϵ_{depo} = Signal under MAS/Signal under static) under MAS too, i.e., the loss of nuclear polarization to electrons via the same CE mechanism under MAS and μw-off condition (Figure 10B).[88] The effect is a manifestation of non-adiabaticity of some *e*-*e* rotor events. Under such conditions, ΔP_e decreases and can lead to nuclear depolarization via reverse nucleus-to-electron CE transfer. The effect becomes severely pronounced as the ratio T_{1e}/τ_r increases, i.e. when a low ΔP_e ($\leq P_n$) is maintained throughout the rotor period.[72,88,89] Since both effects are manifestations of the triple-flip mechanism, we mapped their correlation for 230 different orientations of a *e*-*e*-*n* spin system that is designed to mimic the *e*-*e* coupling strength of the AMUPol radical.[33,67] Similar to the observation made by Mentink-Vigier et al. for TOTAPOL radicals,[89] we find a linear correlation between ϵ_{depo} and the realistic enhancement factor, $\epsilon_{abs} = \epsilon_{on/off} * \epsilon_{depo}$ (marked by the dotted line in Figure 10C). Specific orientations can be beneficial or detrimental in minimizing depolarization and maximizing DNP enhancement. Interestingly, there are some orientations that deviate from the statistical correlation of enhancement vs. depolarization in the powder ensemble, although the sequence of CE and *e*-*e* rotor events are identical in both

enhancement and depolarization processes. This is due to μw events. The time-sequence of the μw events with respect to the other two events determines the DNP enhancement actually accrued. Consequentially, a given orientation can lead to significant depolarization but also have a very high DNP enhancement, as highlighted with the horizontal line in Figure 10C. Interestingly, this suggests that the presence of moderate depolarization ($0.6 < \epsilon_{depo} < 0.8$) can be an indicator of efficient CE DNP activities of bis-nitroxide PAs that have long T_{1e} and optimum relative g-orientations.

6.4 MAS rate dependence of CE DNP

The insights provided by the LZ model explain the complex behavior of the DNP enhancement as a function of the MAS frequency (ν_r). The effective DNP enhancement is an interplay of the number of rotor events per unit time (which increases with ν_r) and their adiabaticity (which decreases with ν_r). As a result, the CE-DNP enhancement for the common AMUPol radical (ϵ_{abs}) sharply increases with ν_r compared to static conditions. The enhancement reaches an optimum, then levels out, and subsequently deteriorates at very fast MAS (Figure 10B). The exact position of this optimum depends on the *e*-*e* coupling strengths, as they determine the adiabaticity of the events. The CE-DNP benefits from the effect of MAS that incorporates a large number of orientations to fulfill the CE polarization transfer condition – an effect dubbed as "self-chirping".[85]

6.5 Design of new μw irradiation scheme

The LZ theory has played a key role for the development of new μw pulse irradiation schemes to achieve efficient DNP with fast $1/T_{1e}$ rates, as detailed earlier and illustrated in Figure 3. The microscopic insights of μw and CE rotor-events under MAS that are separated in time inspired the idea to execute fast and broadband irradiation to maintain a gradient ΔP_e throughout all CE events that occur during sample rotation and result in a larger DNP enhancement. This is elaborated in section 4.3.[54] So far, we demonstrated the importance

of numerical simulations to understand and develop DNP. Next, we highlight the available packages to perform these simulations.

6.6 DNP Numerical Simulation Packages

SpinEvolution (C based) and Spinach (MATLAB based) are two simulation packages that are available for general users to carry out quantum mechanical simulations of DNP effects that incorporate all relevant experimental parameters (including relaxation rates).[90,91] Spinach is a freeware developed by Kuprov and coworkers.[91,92] SpinEvolution was developed by Veshtort et al.[90] and has been commercialized, but is significantly more rapid for DNP simulations compared to Spinach. For example, a typical CE DNP profile (e.g. as shown in Figure 6A) can be computed in a few minutes using SpinEvolution, but may take several hours by Spinach. Of course, the exact simulation duration depends on the magnitude of the different terms in the relevant Hamiltonian describing the spin system, especially of the off-diagonal or the perturbation terms. We used SpinEvolution to carry out numerical simulations in all of our recent studies after the program's functionality was extended to include the capability to simulate DNP phenomena. We found this tool indispensable for simulating and understating effects of the truncated CE and TM DNP mechanism that we observed experimentally, and predicting the characteristics of new bis-nitroxide and mixed radical systems as PAs.[27,33,61,62,66,69,93]

Just as with numerical simulations of other types of NMR experiments, DNP simulations are performed by the numerical integration of the time-dependent Liouville-von Neumann equation of motion. The Hamiltonian (Equation. 3) has the following form in this case:

$$\hat{\mathcal{H}} = \hat{\mathcal{H}}_{\text{Zeeman}} + \hat{\mathcal{H}}_{\rceil-\rceil} + \hat{\mathcal{H}}_{\text{hyperfine}} + \hat{\mathcal{H}}_{\mu\sqsupset} \tag{3}$$

This includes the pseudo-secular ($I_xS_z + I_yS_z$) parts of the hyperfine coupling terms and uses the lab frame for the nuclei I, while a rotating frame is used for the electron spins S.

The electron spin relaxation terms are assumed to be of the form generated by fast random fluctuations of the single-spin operators, having phenomenological relaxation time-constants (T_1 and T_2). The $\mathcal{H}_{\mu w}$ term may have an arbitrary time-dependent frequency and amplitude. Paramagnetic spin systems with effective spin quantum number $S > 1/2$ are allowed in addition to spin 1/2 electrons. Calculations of MAS DNP are particularly challenging because the integration of spin dynamics must be performed in very small-time steps (typically on the order of 10 ns). The situation is further complicated by the incorporation of relaxation in the equation of motion, necessitating calculations in Liouville space, which makes such calculations very expensive compared with conventional MAS ssNMR simulations where pseudo secular terms are ignored and spin interactions are much smaller in magnitude so that their numerical diagonalization is easier. To alleviate this problem SpinEvolution uses a set of algorithms that integrate the equation of motion in such systems much more efficiently than the straightforward methods used by other authors.[85,86] The method set includes the Liouville space, reduced Liouville space and Hilbert space algorithms. The latter methods (although not exact) are useful for dealing with very large spin systems, where calculations in Liouville space become exponentially time consuming. In particular, the method used by Thurber and Tycko[85] is a special case of the SpinEvolution's Hilbert space algorithm. Most recently, Perras and co-worker incorporated the LZ formalism with locally restricted low-level correlations using the Liouville space method that can allow for simulations of systems containing thousands of spins.[94] The method is not exact and truncates the spin interactions to the nearest neighbor, yet it can be very helpful for understanding bulk phenomena such as nuclear spin diffusion in presence of electrons.

7. Conclusion and Outlook

In this review, we have highlighted three approaches to enhance the efficiency of DNP towards its theoretical limit in the experimentally crucial high B0 and fast MAS regimes. Schemes

for microwave irradiation to achieve "smart" manipulation of electron spin coherence or polarization are crucial for future DNP experiments. High power coherent microwave pulses with precise control over the phase, frequency, amplitude and pulse timing can eventually lead to field independent and coherent DNP mechanisms when sufficiently high-power sources (such as gyroamplifiers) become available. In the interim, currently available microwave technology such as AWG concatenated solid state sources can be used to achieve an effective shaping of an electron spin polarization gradient across the EPR spectrum to significantly boost DNP under MAS, especially applied to DNP experiments using mixed narrow and broad line radicals as PAs. Additionally, increasing the effective *e*-*e* coupling in the PAs can improve the triple (e-*e*-*n*) flip based incoherent DNP processes that rely on a coupled multi-electron spin network. While CE is easier to model and is the current method of choice, TM may have superior utility at high B0 and in the fast MAS regime owing to the stronger *e*-*e* coupling network involved.

Meanwhile, the incoherent processes of CE and TM DNP can be diagnosed and optimized with the help of EPR spectroscopy to reveal the dynamics of the coupled electron spin system under operational DNP conditions. Pump-probe ELDOR experiments can directly diagnose the polarization gradient generated by (shaped) μw irradiation; predict the efficiency of triple (*e*-*e*-*n*) flip processes; determine the extent of the *e*-*e* coupling network; and identify characteristic signatures of the underlying DNP mechanisms. Such diagnostic capabilities will be key to rational development of effective high field DNP methods. Such capabilities to diagnose the properties of the coupled electron and nuclear spin network are critical to utilize and apply TM using strongly coupled narrow line radicals that we believe is one of the most promising approaches for DNP.[84]

DNP is a complex process involving a multitude of interconnected parameters and events that occur on nanosecond timescales. As such, it is impossible to individually tune the effect of a single parameter experimentally, e.g., the coupling strength or type (D or J) or the microscopic, time dependent processes that lead to the build-up of bulk DNP enhancements.

However, insight into these factors can be gained from fully quantum mechanical analysis of spin dynamics underlying DNP, which can in turn assist in the design of efficient PAs or new μw pulse schemes to maximize DNP under desirable experimental conditions. Apart from achieving high enhancements, there is a much broader scope of ongoing developments of DNP aided NMR spectroscopy that we did not discuss here, including the effects of e-n decoupling or achieving DNP at higher temperatures.[30] The study of the nuclear spin diffusion barrier and nuclear spin diffusion in the vicinity of the PAs is another important area that this perspective article did not address.[95,96] Shaped manipulations of electron spin populations using high power coherent μw sources may become critical tools towards the development of e-n correlation spectroscopy using NMR as readout method. This is analogous to multi-dimensional NMR experiments that have been developed in the pursuit of enhanced sensitivity, high resolution, as well as selective structural information. Finally, it would be truly insightful to detect EPR under MAS and DNP to directly measure the evolving electron spin polarization gradient. EPR detection in an MAS rotor under MAS is technically challenging, but feasible, and proof of principle studies have already been demonstrated by Zilm and coworkers on the P1 center of a diamond sample (private communication). We assert that advancing DNP requires interdisciplinary expertise and insight, invoking extensive cross-talks and collaborations across different disciplines of research from synthetic chemistry, quantum mechanical modeling, analytical instrument development, and of course electron and nuclear spin magnetic resonance spectroscopy, and hence offers opportunities to push new science beyond amplifying the scope of NMR spectroscopy.

Acknowledgement

This work was supported by the National Science Foundation Grant CHE CMI #2004217. We thank Dr. Mikhail Veshtort for help with SpinEvolution package.

References

(1) Thankamony, A. S. L.; Wittmann, J. J.; Kaushik, M.; Corzilius, B. Dynamic nuclear polarization for sensitivity enhancement in modern solid-state NMR. *Progress in Nuclear Magnetic Resonance Spectroscopy* **2017**, *102-103*, 120 – 195.

(2) Jeon, J.; Thurber, K. R.; Ghirlando, R.; Yau, W.-M.; Tycko, R. Application of millisecond time-resolved solid state NMR to the kinetics and mechanism of melittin self-assembly. *Proceedings of the National Academy of Sciences* **2019**, *116*, 16717–16722.

(3) Potapov, A.; Yau, W.-M.; Ghirlando, R.; Thurber, K. R.; Tycko, R. Successive stages of amyloid-β self-assembly characterized by solid-state nuclear magnetic resonance with dynamic nuclear polarization. *J. Am. Chem. Soc.* **2015**, *137*, 8294–8307.

(4) Wylie, B. J.; Dzikovski, B. G.; Pawsey, S.; Caporini, M.; Rosay, M.; Freed, J. H.; McDermott, A. E. Dynamic nuclear polarization of membrane proteins: covalently bound spin-labels at protein–protein interfaces. *Journal of Biomolecular NMR* **2015**, *61*, 361–367.

(5) Su, Y.; Andreas, L.; Griffin, R. G. Magic Angle Spinning NMR of Proteins: High-Frequency Dynamic Nuclear Polarization and 1H Detection. *Annual Review of Biochemistry* **2015**, *84*, 465–497, PMID: 25839340.

(6) Smith, A. N.; Caporini, M. A.; Fanucci, G. E.; Long, J. R. A Method for Dynamic Nuclear Polarization Enhancement of Membrane Proteins. *Angewandte Chemie International Edition* **2015**, *54*, 1542–1546.

(7) Perras, F. A.; Kobayashi, T.; Pruski, M. Natural abundance 17O DNP two-dimensional and surface-enhanced NMR spectroscopy. *Journal of the American Chemical Society* **2015**, *137*, 8336–8339.

(8) Grüning, W. R.; Rossini, A. J.; Zagdoun, A.; Gajan, D.; Lesage, A.; Emsley, L.; Copéret, C. Molecular-level characterization of the structure and the surface chemistry of periodic mesoporous organosilicates using DNP-surface enhanced NMR spectroscopy. *Physical Chemistry Chemical Physics* **2013**, *15*, 13270–13274.

(9) Lafon, O.; Thankamony, A. S. L.; Rosay, M.; Aussenac, F.; Lu, X.; Trébosc, J.; Bout-Roumazeilles, V.; Vezin, H.; Amoureux, J.-P. Indirect and direct 29 Si dynamic nuclear polarization of dispersed nanoparticles. *Chemical Communications* **2013**, *49*, 2864–2866.

(10) Wolf, T.; Kumar, S.; Singh, H.; Chakrabarty, T.; Aussenac, F.; Frenkel, A. I.; Major, D. T.; Leskes, M. Endogenous dynamic nuclear polarization for natural abundance 17O and lithium NMR in the bulk of inorganic solids. *Journal of the American Chemical Society* **2018**, *141*, 451–462.

(11) Lafon, O.; Thankamony, A. S. L.; Kobayashi, T.; Carnevale, D.; Vitzthum, V.; Slowing, I. I.; Kandel, K.; Vezin, H.; Amoureux, J.-P.; Bodenhausen, G., et al. Mesoporous silica nanoparticles loaded with surfactant: low temperature magic angle spinning 13C and 29Si NMR enhanced by dynamic nuclear polarization. *The Journal of Physical Chemistry C* **2013**, *117*, 1375–1382.

(12) Berruyer, P.; Emsley, L.; Lesage, A. DNP in materials science: touching the surface. *Emagres* **2007**, 93–104.

(13) Nagashima, H.; Trebosc, J.; Kon, Y.; Sato, K.; Lafon, O.; Amoureux, J.-P. Observation of low-γ quadrupolar nuclei by surface-enhanced NMR spectroscopy. *Journal of the American Chemical Society* **2020**,

(14) Lesage, A.; Lelli, M.; Gajan, D.; Caporini, M. A.; Vitzthum, V.; Miéville, P.; Alauzun, J.; Roussey, A.; Thieuleux, C.; Mehdi, A., et al. Surface enhanced NMR

spectroscopy by dynamic nuclear polarization. *Journal of the American Chemical Society* **2010**, *132*, 15459–15461.

(15) Lelli, M.; Gajan, D.; Lesage, A.; Caporini, M. A.; Vitzthum, V.; Miéville, P.; Héroguel, F.; Rascón, F.; Roussey, A.; Thieuleux, C., et al. Fast characterization of functionalized silica materials by silicon-29 surface-enhanced NMR spectroscopy using dynamic nuclear polarization. *Journal of the American Chemical Society* **2011**, *133*, 2104–2107.

(16) Vitzthum, V.; Miéville, P.; Carnevale, D.; Caporini, M. A.; Gajan, D.; Copéret, C.; Lelli, M.; Zagdoun, A.; Rossini, A. J.; Lesage, A., et al. Dynamic nuclear polarization of quadrupolar nuclei using cross polarization from protons: surface-enhanced aluminium-27 NMR. *Chemical Communications* **2012**, *48*, 1988–1990.

(17) Aladin, V.; Vogel, M.; Binder, R.; Burghardt, I.; Suess, B.; Corzilius, B. Complex Formation of the Tetracycline-Binding Aptamer Investigated by Specific Cross-Relaxation under DNP. *Angewandte Chemie International Edition* **2019**, *58*, 4863–4868.

(18) Rogawski, R.; Sergeyev, I. V.; Li, Y.; Ottaviani, M. F.; Cornish, V.; McDermott, A. E. Dynamic Nuclear Polarization Signal Enhancement with High-Affinity Biradical Tags. *The Journal of Physical Chemistry B* **2017**, *121*, 1169–1175, PMID: 28099013.

(19) Carver, T. R.; Slichter, C. P. Polarization of Nuclear Spins in Metals. *Phys. Rev.* **1953**, *92*, 212–213.

(20) Hovav, Y.; Feintuch, A.; Vega, S. Theoretical aspects of dynamic nuclear polarization in the solid state–the solid effect. *Journal of Magnetic Resonance* **2010**, *207*, 176–189.

(21) Hovav, Y.; Feintuch, A.; Vega, S. Theoretical aspects of dynamic nuclear polarization in the solid state–the cross effect. *Journal of Magnetic Resonance* **2012**, *214*, 29–41.

(22) Wenckebach, W. T. Dynamic nuclear polarization via the cross effect and thermal mixing: A. The role of triple spin flips. *Journal of Magnetic Resonance* **2019**, *299*, 124–134.

(23) Jähnig, F.; Himmler, A.; Kwiatkowski, G.; Däpp, A.; Hunkeler, A.; Kozerke, S.; Ernst, M. A spin-thermodynamic approach to characterize spin dynamics in TEMPO-based samples for dissolution DNP at 7 T field. *Journal of Magnetic Resonance* **2019**, *303*, 91–104.

(24) Zagdoun, A.; Casano, G.; Ouari, O.; Schwarzwälder, M.; Rossini, A. J.; Aussenac, F.; Yulikov, M.; Jeschke, G.; Coperet, C.; Lesage, A., et al. Large molecular weight nitroxide biradicals providing efficient dynamic nuclear polarization at temperatures up to 200 K. *Journal of the American Chemical Society* **2013**, *135*, 12790–12797.

(25) Mathies, G.; Caporini, M. A.; Michaelis, V. K.; Liu, Y.; Hu, K.-N.; Mance, D.; Zweier, J. L.; Rosay, M.; Baldus, M.; Griffin, R. G. Efficient dynamic nuclear polarization at 800 MHz/527 GHz with trityl-nitroxide biradicals. *Angewandte Chemie International Edition* **2015**, *54*, 11770–11774.

(26) Wisser, D.; Karthikeyan, G.; Lund, A.; Casano, G.; Karoui, H.; Yulikov, M.; Menzildjian, G.; Pinon, A. C.; Purea, A.; Engelke, F., et al. BDPA-nitroxide biradicals tailored for efficient dynamic nuclear polarization enhanced solid-state NMR at magnetic fields up to 21.1 T. *Journal of the American Chemical Society* **2018**, *140*, 13340–13349.

(27) Li, Y.; Equbal, A.; Tagami, K.; Han, S. Electron spin density matching for cross-effect dynamic nuclear polarization. *Chemical Communications* **2019**, *55*, 7591–7594.

(28) Mentink-Vigier, F.; Marin-Montesinos, I.; Jagtap, A. P.; Halbritter, T.; Van Tol, J.; Hediger, S.; Lee, D.; Sigurdsson, S. T.; Gaël, D. P. Computationally assisted design of polarizing agents for dynamic nuclear polarization enhanced NMR: the AsymPol family. *Journal of the American Chemical Society* **2018**, *140*, 11013–11019.

(29) Leavesley, A.; Jain, S.; Kamniker, I.; Zhang, H.; Rajca, S.; Rajca, A.; Han, S. Maximizing NMR signal per unit time by facilitating the e–e–n cross effect DNP rate. *Physical Chemistry Chemical Physics* **2018**, *20*, 27646–27657.

(30) Lelli, M.; Chaudhari, S. R.; Gajan, D.; Casano, G.; Rossini, A. J.; Ouari, O.; Tordo, P.; Lesage, A.; Emsley, L. Solid-state dynamic nuclear polarization at 9.4 and 18.8 T from 100 K to room temperature. *Journal of the American Chemical Society* **2015**, *137*, 14558–14561.

(31) Lund, A.; Casano, G.; Menzildjian, G.; Kaushik, M.; Stevanato, G.; Yulikov, M.; Jabbour, R.; Wisser, D.; Renom-Carrasco, M.; Thieuleux, C., et al. TinyPols: a family of water-soluble binitroxides tailored for dynamic nuclear polarization enhanced NMR spectroscopy at 18.8 and 21.1 T. *Chemical Science* **2020**, *11*, 2810–2818.

(32) Berruyer, P.; Björgvinsdottir, S.; Bertarello, A.; Stevanato, G.; Rao, Y.; Karthikeyan, G.; Casano, G.; Ouari, O.; Lelli, M.; Reiter, C., et al. Dynamic nuclear polarization enhancement of 200 at 21.15 T enabled by 65 kHz magic angle spinning. *The Journal of Physical Chemistry Letters* **2020**, *11*, 8386–8391.

(33) Equbal, A.; Tagami, K.; Han, S. Balancing dipolar and exchange coupling in biradicals to maximize cross effect dynamic nuclear polarization. *Physical Chemistry Chemical Physics* **2020**, *22*, 13569–13579.

(34) Scott, F. J.; Saliba, E. P.; Albert, B. J.; Alaniva, N.; Sesti, E. L.; Gao, C.; Golota, N. C.; Choi, E. J.; Jagtap, A. P.; Wittmann, J. J.; Eckardt, M.; Harneit, W.; Corzilius, B.; Th. Sigurdsson, S.; Barnes, A. B. Frequency-agile gyrotron for electron decoupling and pulsed dynamic nuclear polarization. *Journal of Magnetic Resonance* **2018**, *289*, 45–54.

(35) Judge, P. T.; Sesti, E. L.; Alaniva, N.; Saliba, E. P.; Price, L. E.; Gao, C.; Halbritter, T.; Sigurdsson, S. T.; Kyei, G. B.; Barnes, A. B. Characterization of frequency-chirped

dynamic nuclear polarization in rotating solids. *Journal of Magnetic Resonance* **2020**, *313*, 106702.

(36) Takahashi, S.; Brunel, L.-C.; Edwards, D. T.; van Tol, J.; Ramian, G.; Han, S.; Sherwin, M. S. Pulsed electron paramagnetic resonance spectroscopy powered by a free-electron laser. *Nature* **2012**, *489*, 409–413.

(37) Kaminker, I.; Barnes, R.; Han, S. Arbitrary waveform modulated pulse EPR at 200GHz. *Journal of Magnetic Resonance* **2017**, *279*, 81–90.

(38) Soane, A. V.; Shapiro, M. A.; Jawla, S.; Temkin, R. J. Operation of a 140-GHz Gyro-Amplifier Using a Dielectric-Loaded, Severless Confocal Waveguide. *IEEE Transactions on Plasma Science* **2017**, *45*, 2835–2840.

(39) Kemp, T. F.; Dannatt, H. R.; Barrow, N. S.; Watts, A.; Brown, S. P.; Newton, M. E.; Dupree, R. Dynamic nuclear polarization enhanced NMR at 187 GHz/284 MHz using an extended interaction Klystron amplifier. *Journal of Magnetic Resonance* **2016**, *265*, 77–82.

(40) Nevzorov, A. A.; Milikisiyants, S.; Marek, A. N.; Smirnov, A. I. Multi-resonant photonic band-gap/saddle coil DNP probehead for static solid state NMR of microliter volume samples. *Journal of Magnetic Resonance* **2018**, *297*, 113 – 123.

(41) Purea, A.; Reiter, C.; Dimitriadis, A. I.; de Rijk, E.; Aussenac, F.; Sergeyev, I.; Rosay, M.; Engelke, F. Improved waveguide coupling for 1.3 mm MAS DNP probes at 263 GHz. *Journal of Magnetic Resonance* **2019**, *302*, 43–49.

(42) Brunner, H.; Fritsch, R.; Hausser, K. Cross polarization in electron nuclear double resonance by satisfying the Hartmann-Hahn condition. *Zeitschrift für Naturforschung A* **1987**, *42*, 1456–1457.

(43) Henstra, A.; Dirksen, P.; Wenckebach, W. T. Enhanced dynamic nuclear polarization by the integrated solid effect. *Physics Letters A* **1988**, *134*, 134–136.

(44) Can, T. V.; Walish, J. J.; Swager, T. M.; Griffin, R. G. Time domain DNP with the NOVEL sequence. *The Journal of Chemical Physics* **2015**, *143*, 054201.

(45) Mathies, G.; Jain, S.; Reese, M.; Griffin, R. G. Pulsed Dynamic Nuclear Polarization with Trityl Radicals. *The Journal of Physical Chemistry Letters* **2016**, *7*, 111–116, PMID: 26651876.

(46) Jain, S. K.; Mathies, G.; Griffin, R. G. Off-resonance NOVEL. *The Journal of chemical physics* **2017**, *147*, 164201.

(47) Tan, K. O.; Yang, C.; Weber, R. T.; Mathies, G.; Griffin, R. G. Time-optimized pulsed dynamic nuclear polarization. *Science advances* **2019**, *5*, eaav6909.

(48) Tan, K. O.; Jawla, S.; Temkin, R. J.; Griffin, R. G. Pulsed Dynamic Nuclear Polarization. *eMagRes* **2019**, 339–352.

(49) Nanni, E. A.; Jawla, S.; Lewis, S. M.; Shapiro, M. A.; Temkin, R. J. Photonic-band-gap gyrotron amplifier with picosecond pulses. *Applied Physics Letters* **2017**, *111*, 233504.

(50) Thumm, M. State-of-the-Art of High-Power Gyro-Devices and Free Electron Masers. *Journal of Infrared, Millimeter, and Terahertz Waves* **2020**, *41*, 1–140.

(51) Hovav, Y.; Feintuch, A.; Vega, S.; Goldfarb, D. Dynamic nuclear polarization using frequency modulation at 3.34 T. *Journal of Magnetic Resonance* **2014**, *238*.

(52) Bornet, A.; Milani, J.; Vuichoud, B.; Perez Linde, A. J.; Bodenhausen, G.; Jannin, S. Microwave frequency modulation to enhance Dissolution Dynamic Nuclear Polarization Dedicated to To Martial Rey, as a token of appreciation. *Chemical Physics Letters* **2014**, *602*, 63–67.

(53) Kaminker, I.; Barnes, R.; Han, S. Arbitrary waveform modulated pulse EPR at 200 GHz. *Journal of Magnetic Resonance* **2017**, *279*, 81–90.

(54) Equbal, A.; Tagami, K.; Han, S. Pulse-Shaped Dynamic Nuclear Polarization under Magic-Angle Spinning. *Journal of Physical Chemistry Letters* **2019**, *10*, 7781–7788.

(55) Alaniva, N.; Saliba, E. P.; Sesti, E. L.; Judge, P. T.; Barnes, A. B. Electron Decoupling with Chirped Microwave Pulses for Rapid Signal Acquisition and Electron Saturation Recovery. *Angewandte Chemie International Edition* **2019**, *58*, 7259–7262.

(56) Gao, C.; Alaniva, N.; Saliba, E. P.; Sesti, E. L.; Judge, P. T.; Scott, F. J.; Halbritter, T.; Sigurdsson, S. T.; Barnes, A. B. Frequency-chirped dynamic nuclear polarization with magic angle spinning using a frequency-agile gyrotron. *Journal of Magnetic Resonance* **2019**, *308*, 106586.

(57) Hu, K.-N.; Bajaj, V. S.; Rosay, M.; Griffin, R. G. High-frequency dynamic nuclear polarization using mixtures of TEMPO and trityl radicals. *The Journal of chemical physics* **2007**, *126*, 044512.

(58) Karabanov, A.; Kwiatkowski, G.; Perotto, C. U.; Wiśniewski, D.; McMaster, J.; Lesanovsky, I.; Köckenberger, W. Dynamic nuclear polarisation by thermal mixing: quantum theory and macroscopic simulations. *Physical Chemistry Chemical Physics* **2016**, *18*, 30093–30104.

(59) Guarin, D.; Marhabaie, S.; Rosso, A.; Abergel, D.; Bodenhausen, G.; Ivanov, K. L.; Kurzbach, D. Characterizing thermal mixing dynamic nuclear polarization via cross-talk between spin reservoirs. *The journal of physical chemistry letters* **2017**, *8*, 5531–5536.

(60) Wenckebach, W. T. Spectral diffusion and dynamic nuclear polarization: Beyond the high temperature approximation. *Journal of Magnetic Resonance* **2017**, *284*, 104–114.

(61) Equbal, A.; Li, Y.; Tabassum, T.; Han, S. Crossover from Solid Effect to Thermal Mixing 1H Dynamic Nuclear Polarization in Trityl-OX063. *The Journal of Physical Chemistry Letters* **2020**,

(62) Li, Y.; Equbal, A.; Tabassum, T.; Han, S. 1H Thermal Mixing Dynamic Nuclear Polarization with BDPA as Polarizing Agents. *The Journal of Physical Chemistry Letters* **2020**, *11*, 9195–9202.

(63) Bornet, A.; Pinon, A.; Jhajharia, A.; Baudin, M.; Ji, X.; Emsley, L.; Bodenhausen, G.; Ardenkjaer-Larsen, J. H.; Jannin, S. Microwave-gated dynamic nuclear polarization. *Physical Chemistry Chemical Physics* **2016**, *18*, 30530–30535.

(64) Jain, S. K.; Siaw, T. A.; Equbal, A.; Wilson, C. B.; Kaminker, I.; Han, S. Reversal of Paramagnetic Effects by Electron Spin Saturation. *The Journal of Physical Chemistry C* **2018**, *122*, 5578–5589.

(65) Leavesley, A.; Wilson, C. B.; Sherwin, M.; Han, S. Effect of water/glycerol polyhysRevLett.18.110morphism on dynamic nuclear polarization. *Physical Chemistry Chemical Physics* **2018**, *20*, 9897–9903.

(66) Equbal, A.; Li, Y.; Leavesley, A.; Huang, S.; Rajca, S.; Rajca, A.; Han, S. Truncated Cross Effect Dynamic Nuclear Polarization: An Overhauser Effect Doppelgänger. *The journal of physical chemistry letters* **2018**, *9*, 2175–2180.

(67) Gast, P.; Mance, D.; Zurlo, E.; Ivanov, K. L.; Baldus, M.; Huber, M. A tailored multifrequency EPR approach to accurately determine the magnetic resonance parameters of dynamic nuclear polarization agents: application to AMUPol. *Physical Chemistry Chemical Physics* **2017**, *19*, 3777–3781.

(68) Soetbeer, J.; Gast, P.; Walish, J. J.; Zhao, Y.; George, C.; Yang, C.; Swager, T. M.; Griffin, R. G.; Mathies, G. Conformation of bis-nitroxide polarizing agents by multi-

frequency EPR spectroscopy. *Physical Chemistry Chemical Physics* **2018**, *20*, 25506–25517.

(69) Tagami, K.; Equbal, A.; Kaminker, I.; Kirtman, B.; Han, S. Biradical rotamer states tune electron J coupling and MAS dynamic nuclear polarization enhancement. *Solid state nuclear magnetic resonance* **2019**, *101*, 12–20.

(70) Zhai, W.; Feng, Y.; Liu, H.; Rockenbauer, A.; Mance, D.; Li, S.; Song, Y.; Baldus, M.; Liu, Y. Diastereoisomers of L-proline-linked trityl-nitroxide biradicals: synthesis and effect of chiral configurations on exchange interactions. *Chemical science* **2018**, *9*, 4381–4391.

(71) Kubicki, D. J.; Casano, G.; Schwarzwälder, M.; Abel, S.; Sauvée, C.; Ganesan, K.; Yulikov, M.; Rossini, A. J.; Jeschke, G.; Copéret, C.; Lesage, A.; Tordo, P.; Ouari, O.; Emsley, L. Rational design of dinitroxide biradicals for efficient cross-effect dynamic nuclear polarization. *Chemical science* **2016**, *7*, 550–558.

(72) Lund, A.; Equbal, A.; Han, S. Tuning nuclear depolarization under MAS by electron T 1e. *Physical Chemistry Chemical Physics* **2018**, *20*, 23976–23987.

(73) Weber, E.; Vezin, H.; Kempf, J.; Bodenhausen, G.; Abergél, D.; Kurzbach, D. Anisotropic longitudinal electronic relaxation affects DNP at cryogenic temperatures. *Physical Chemistry Chemical Physics* **2017**, *19*, 16087–16094.

(74) Leavesley, A.; Shimon, D.; Siaw, T. A.; Feintuch, A.; Goldfarb, D.; Vega, S.; Kaminker, I.; Han, S. Effect of electron spectral diffusion on static dynamic nuclear polarization at 7 Tesla. *Physical Chemistry Chemical Physics* **2017**, *19*, 3596–3605.

(75) Hovav, Y.; Shimon, D.; Kaminker, I.; Feintuch, A.; Goldfarb, D.; Vega, S. Effects of the electron polarization on dynamic nuclear polarization in solids. *Physical Chemistry Chemical Physics* **2015**, *17*, 6053–6065.

(76) Hovav, Y.; Feintuch, A.; Vega, S.; Goldfarb, D. Dynamic nuclear polarization using frequency modulation at 3.34 T. *Journal of Magnetic Resonance* **2014**, *238*, 94–105.

(77) Kundu, K.; Feintuch, A.; Vega, S. Theoretical Aspects of the Cross Effect Enhancement of Nuclear Polarization under Static Dynamic Nuclear Polarization Conditions. *The journal of physical chemistry letters* **2019**, *10*, 1769–1778.

(78) Can, T. V.; Caporini, M. A.; Mentink-Vigier, F.; Corzilius, B.; Walish, J. J.; Rosay, M.; Maas, W. E.; Baldus, M.; Vega, S.; Swager, T. M.; Griffin, R. G. Overhauser effects in insulating solids. *The Journal of Chemical Physics* **2014**, *141*, 064202.

(79) Ji, X.; Can, T.; Mentink-Vigier, F.; Bornet, A.; Milani, J.; Vuichoud, B.; Caporini, M.; Griffin, R. G.; Jannin, S.; Goldman, M., et al. Overhauser effects in non-conducting solids at 1.2 K. *Journal of Magnetic Resonance* **2018**, *286*, 138–142.

(80) Griffin, R.; Prisner, T. High field dynamic nuclear polarization—the renaissance. *Physical Chemistry Chemical Physics* **2010**, *12*, 5737–5740.

(81) Mentink-Vigier, F.; Vega, S.; De Paëpe, G. Fast and accurate MAS–DNP simulations of large spin ensembles. *Physical Chemistry Chemical Physics* **2017**, *19*, 3506–3522.

(82) Mentink-Vigier, F.; Barra, A.-L.; Van Tol, J.; Hediger, S.; Lee, D.; De Paëpe, G. De novo prediction of cross-effect efficiency for magic angle spinning dynamic nuclear polarization. *Physical Chemistry Chemical Physics* **2019**, *21*, 2166–2176.

(83) Perras, F. A.; Sadow, A.; Pruski, M. In silico design of DNP polarizing agents: can current dinitroxides be improved? *ChemPhysChem* **2017**, *18*, 2279–2287.

(84) Equbal, A.; Leavesley, A.; Jain, S. K.; Han, S. Cross-effect dynamic nuclear polarization explained: polarization, depolarization, and oversaturation. *The journal of physical chemistry letters* **2019**, *10*, 548–558.

(85) Thurber, K. R.; Tycko, R. Theory for cross effect dynamic nuclear polarization under magic-angle spinning in solid state nuclear magnetic resonance: the importance of level crossings. *The Journal of chemical physics* **2012**, *137*, 084508.

(86) Mentink-Vigier, F.; Akbey, Ü.; Oschkinat, H.; Vega, S.; Feintuch, A. Theoretical aspects of magic angle spinning-dynamic nuclear polarization. *Journal of Magnetic Resonance* **2015**, *258*, 102–120.

(87) Rodin, B. A.; Ivanov, K. L. Representation of population exchange at level anti-crossings. *Magnetic Resonance Discussions* **2020**, 1–26.

(88) Thurber, K. R.; Tycko, R. Perturbation of nuclear spin polarizations in solid state NMR of nitroxide-doped samples by magic-angle spinning without microwaves. *The Journal of chemical physics* **2014**, *140*, 05B608_1.

(89) Mentink-Vigier, F.; Paul, S.; Lee, D.; Feintuch, A.; Hediger, S.; Vega, S.; De Paëpe, G. Nuclear depolarization and absolute sensitivity in magic-angle spinning cross effect dynamic nuclear polarization. *Physical Chemistry Chemical Physics* **2015**, *17*, 21824–21836.

(90) Veshtort, M.; Griffin, R. G. SPINEVOLUTION: a powerful tool for the simulation of solid and liquid state NMR experiments. *Journal of Magnetic Resonance* **2006**, *178*, 248–282.

(91) Hogben, H.; Krzystyniak, M.; Charnock, G.; Hore, P.; Kuprov, I. Spinach–a software library for simulation of spin dynamics in large spin systems. *Journal of Magnetic Resonance* **2011**, *208*, 179–194.

(92) Karabanov, A.; van der Drift, A.; Edwards, L. J.; Kuprov, I.; Köckenberger, W. Quantum mechanical simulation of solid effect dynamic nuclear polarisation using Krylov–Bogolyubov time averaging and a restricted state-space. *Physical Chemistry Chemical Physics* **2012**, *14*, 2658–2668.

(93) Lund, A.; Equbal, A.; Han, S. Tuning nuclear depolarization under MAS by electron T1e. *Physical Chemistry Chemical Physics* **2018**, *20*, 23976–23987.

(94) Perras, F. A.; Raju, M.; Carnahan, S. L.; Akbarian, D.; Van Duin, A. C.; Rossini, A. J.; Pruski, M. Full-Scale Ab Initio Simulation of Magic-Angle-Spinning Dynamic Nuclear Polarization. *The Journal of Physical Chemistry Letters* **2020**, *11*, 5655–5660.

(95) Jain, S. K.; Yu, C.-J.; Wilson, C. B.; Tabassum, T.; Freedman, D. E.; Han, S. Dynamic Nuclear Polarization with Vanadium (IV) Metal Centers. *Chem* **2021**, *7*, 421–435.

(96) Prisco, N. A.; Pinon, A. C.; Emsley, L.; Chmelka, B. F. Scaling analyses for hyperpolarization transfer across a spin-diffusion barrier and into bulk solid media. *Physical Chemistry Chemical Physics* **2021**, *23*, 1006–1020.

Abbreviations

DNP: dynamic nuclear polarization

NMR: nuclear magnetic resonance

EPR: electron paramagnetic resonance

PA: polarizing agent

e: electron spin

n: nuclear spin

MAS: magic angle spinning

μw: microwave

SE: solid effect

CE: cross effect

OE: Overhauser effect

TM: thermal mixing

DNP-SENS: DNP-Surface Enhanced NMR Spectroscopy

$T_1(^1\mathrm{H})$: proton spin-lattice relaxation

CP: cross-polarization

RF: radio frequency

γ: gyromagnetic ratio

DQ: double quantum

ZQ: zero quantum

ω_e : electron Larmor frequency

ω_{0n} : nuclear Larmor frequency

Pe: electron spin polarization

ω_{ee} : electron-electron coupling strength

D: dipolar coupling

J: exchange coupling

FEL: free electron laser

VCO: voltage-controlled oscillator

AMC: amplifier multiplier chain

AWG: arbitrary waveform generator

NOVEL: Nuclear Orientation Via Electron-spin Locking

TOP: time-optimized μw pulse

CW: continuous wave

FM: frequency modulation

T_{1e}: electron spin-lattice relaxation

T_{2e} : electron spin-spin relaxation

τ_r : magic-angle spinning rotor period

eSD: electron spectral diffusion

ELDOR: electron-electron double resonance

$\epsilon(^1H)$: ^{1}H DNP enhancement

$\epsilon_{on/off}$: nuclear enhancement factor calculated as ratio of NMR signal under μw-on and -off condition

ϵ_{depo} : nuclear depolarization factor calculated as ratio of NMR signal under MAS and static, without μw irradiation

ϵ_{abs} : Absolute nuclear enhancement taking the depolarization factor into account.

Graphical TOC Entry